Near-term impacts of climate variability and change on hydrological systems in West and Central Africa

Sidibe, M., Dieppois, B., Eden, J., Mahé, G., Paturel, J-E., Amoussou, E., Anifowose, B., Van De Wiel, M. & Lawler, D.

Original citation & hyperlink:
Sidibe, M, Dieppois, B, Eden, J, Mahé, G, Paturel, J-E, Amoussou, E, Anifowose, B, Van De Wiel, M & Lawler, D 2020, 'Near-term impacts of climate variability and change on hydrological systems in West and Central Africa', Climate Dynamics, vol. 54, no. 3-4, pp. 2041-2070.

DOI 10.1007/s00382-019-05102-7
ISSN 0930-7575
ESSN 1432-0894

Publisher: Springer

The final publication is available at Springer via http://dx.doi.org/10.1007/s00382-019-05102-7

Climate Dynamics

Near-term impacts of climate variability and change on hydrological systems in West and Central Africa

--Manuscript Draft--

Manuscript Number:	CLDY-D-19-00353R1
Full Title:	Near-term impacts of climate variability and change on hydrological systems in West and Central Africa
Article Type:	Original Article
Keywords:	Climate Change; Hydroclimatic variability; rainfall-runoff modelling; streamflow projections; RCP4.5 scenario; West and Central Africa
Corresponding Author:	Moussa Sidibe, M Sc Coventry University Coventry, England UNITED KINGDOM
Corresponding Author Secondary Information:	
Corresponding Author's Institution:	Coventry University
Corresponding Author's Secondary Institution:	
First Author:	Moussa Sidibe, M Sc
First Author Secondary Information:	
Order of Authors:	Moussa Sidibe, M Sc
	Bastien Dieppois, Ph.D
	Jonathan Eden, Ph.D
	Gil Mahé, Ph.D
	Jean-Emmanuel Paturel, Ph.D
	Ernest Amoussou, Ph.D
	Babatunde Anifowose, Ph.D
	Marco Van De Wiel, Ph.D
	Damian Lawler, Prof.
Order of Authors Secondary Information:	
Funding Information:	
Abstract:	Climate change is expected to significantly impact on the availability of water resources in West and Central Africa through changes in rainfall, temperature and evapotranspiration. Understanding these changes in this region, where surface water is fundamental for economic activity and ecosystem services, is of paramount importance. In this study, we examine the potential impacts of climate variability and change on hydrological systems by the mid-21st century in West and Central Africa, as well as the uncertainties in the different climate-impact modelling pathways. Simulations from nine global climate models downscaled using the Rossby Centre Regional Climate model (RCA4) are evaluated and subsequently bias-corrected using a nonparametric trend-preserving quantile mapping approach. We then use two conceptual hydrological models (GR2M and IHACRES), and a regression-based model built upon multi-timescale sea surface temperatures and streamflow teleconnections, to understand hydrological processes at the subcontinental scale and provide hydrological predictions for the near-term future (2020-2050) under the RCP4.5 emission scenario. The results highlight a zonal contrast in future precipitation between western (dry) and eastern (wet) Sahel, and a robust signal in rising temperature, suggesting an increase

	in potential evapotranspiration, across the multi-model ensemble. Overall, across the region, a significant increase in discharge (~+5%) is expected by the mid-21st century, albeit with high uncertainties reported over most of Central Equatorial Africa inherent to climate models and gridded observation data quality. Interestingly, in this region, teleconnections-based regression models tend to be an alternative to hydrological models.

Near-term impacts of climate variability and change on hydrological systems in West and Central Africa

Moussa Sidibe[1], Bastien Dieppois[1, 2, 3], Jonathan Eden[1], Gil Mahé[4], Jean-Emmanuel Paturel[4], Ernest Amoussou[5], Babatunde Anifowose[6], Marco Van De Wiel[1], Damian Lawler[1]

[1]Centre for Agroecology, Water and Resilience (CAWR), Coventry University, Coventry, UK

[2] Department of Oceanography, University of Cape Town, Cape Town, South Africa

[3] School of Geography, Earth and Environmental Sciences, University of Birmingham, Birmingham, UK

[4] HydroSciences Montpellier (HSM), IRD, Montpellier, France

[5] Département de Géographie et Aménagement du Territoire (DGAT), Université de Parakou, Parakou, Benin

[6]School of Energy, Construction & Environment, Coventry University, UK

Correspondence to: Moussa SIDIBE, Centre for Agroecology, Water and Resilience (CAWR), Coventry University, Ryton Gardens, Ryton on Dunsmore, Coventry, CV8 3LG, UK. **e-mail: moussa.sidibe01@gmail.com**

Abstract

Climate change is expected to significantly impact on the availability of water resources in West and Central Africa through changes in rainfall, temperature and evapotranspiration. Understanding these changes in this region, where surface water is fundamental for economic activity and ecosystem services, is of paramount importance. In this study, we examine the potential impacts of climate variability and change on hydrological systems by the mid-21st century in West and Central Africa, as well as the uncertainties in the different climate-impact modelling pathways. Simulations from nine global climate models downscaled using the Rossby Centre Regional Climate model (RCA4) are evaluated and subsequently bias-corrected using a nonparametric trend-preserving quantile mapping approach. We then use two conceptual hydrological models (GR2M and IHACRES), and a regression-based model built upon multi-timescale sea surface temperatures and streamflow teleconnections, to understand hydrological processes at the subcontinental scale and provide hydrological predictions for the near-term future (2020-2050) under the RCP4.5 emission scenario.

The results highlight a zonal contrast in future precipitation between western (dry) and eastern (wet) Sahel, and a robust signal in rising temperature, suggesting an increase in potential evapotranspiration, across the multi-model ensemble. Overall, across the region, a significant increase in discharge (~+5%) is expected by the mid-21st century, albeit with high uncertainties reported over most of Central Equatorial Africa inherent to climate models and gridded observation data quality. Interestingly, in this region, teleconnections-based regression models tend to be an alternative to hydrological models.

Keywords: *Climate change, Hydroclimatic variability, rainfall-runoff modelling, streamflow projections, RCP4.5 scenario, West and Central Africa.*

1. INTRODUCTION

In Sub-Saharan Africa, more than 60% of the population relies heavily on rainfed agriculture and surface water to sustain a living. This part of the world is identified as one of the most vulnerable to climate change (IPCC 2014; Serdeczny et al. 2017). In particular, the increased risk of droughts and floods, predicted to result from global warming (*e.g.* Aich et al. 2014), is very likely to have severe implications for both natural and human systems. Development of adaptation strategies to adequately tackle the harmful effects of climate change on water resource availability, food production and ecosystem services is one of the most important challenges faced in Sub-Saharan Africa (*e.g.* Aloysius et al. 2016). Such adaptation strategies depend on reliable climate change scenarios and a good representation of different hydrological processes. Climate impacts on hydrological systems are often investigated through a modelling chain whereby outputs of different climate models under different greenhouse gases emission scenarios are used as inputs for hydrological models (*e.g.* Clark et al. 2016; Hattermann et al. 2018). This process however is limited, particularly by the quality of observational datasets and the uncertainties introduced at both the climate (*e.g.* Yira et al. 2017) and hydrological modelling steps (*e.g.* Steinschneider et al. 2015; Kauffeldt et al. 2016; Clark et al. 2016; Giuntoli et al. 2018).

Despite significant advances in climate modelling, both global climate models (GCMs) and regional climate models (RCMs) exhibit important biases in their characterization of West and Central Africa hydroclimatic variability (*e.g.* Druyan et al. 2010; Nikulin et al. 2012, Salack et al. 2015; Aloysius et al. 2016; Mba et al. 2018), which is primarily driven by the West African Monsoon (WAM) system. Biases in climate change scenarios, which are more pronounced in precipitation than temperature trends (*e.g.* Aloysius et al. 2016; Yira et al. 2017) over this region, arise from multiple sources: (1) the influence of climate forcings or unrealistic large-scale variability; (2) poor representation of internal variability; and (3) imperfections in parameterization schemes and unresolved subgrid-scale orography (Eden et al., 2012). For such scenarios to contribute effectively to climate change impact assessment, model biases must be quantified, communicated and, if possible, corrected. Interestingly, projections for the near-term climate which is defined in the fifth assessment report of the Intergovernmental Panel on Climate Change (IPCC) as the period from present through mid-century (IPCC 2013), tend to be less sensitive to uncertainties related to Representative Concentration Pathways (RCP) scenarios (Hawkins and Sutton 2009; IPCC 2013). Over West Africa, for instance, Sylla et al. (2016) found that temperature changes from two forcing scenarios (RCP4.5 & RCP8.5) start to diverge only around 2050.

Previous work has demonstrated the benefit of multi-model approaches in accounting for uncertainties in hydroclimatic scenarios (e.g. Déqué et al. 2007). However, relatively few studies have considered multi-model ensembles for impact assessment at the scale of Sub-Saharan Africa (*e.g.* Mbaye et al. 2015; Oyerinde et al. 2016; Yira et al. 2017). Even in the case that this approach successfully accounts for climate model-related uncertainties, realistic hydrological simulations still require a postprocessing step to remove systematic bias and satisfactorily reproduce seasonal cycles of hydroclimate variables. So-called bias correction algorithms (*e.g.* Maraun et al. 2010; Teutschbein and Seibert 2012; Yira et al. 2017) are often associated with an additional source of uncertainty whose impacts are increasing with the length of the projection lead-time (Hingray and Said 2014). In the context of hydrological climate change impact studies, nonparametric quantile mapping bias correction approaches appear more appropriate, as they can be applied without specific assumptions regarding the nature of the underlying statistical distribution (Gudmundsson et al. 2012). However, some of these methods, despite preserving trends in long-term mean states, result in erroneous trends in extreme quantiles (Cannon et al. 2015). It is therefore important that physical consistency and climate model sensitivity are not altered by bias correction (Hempel et al. 2013). While some studies (*e.g.* Bürger et al. 2011; Cannon, 2016) highlighted the importance of multi-variate quantile mapping, Wilcke et al. (2013) found that univariate quantile mapping induces very little change to the inter-variable linear dependence structure.

Hydrological model uncertainty, while in general lesser than climate model uncertainty, ought to be also accounted for in climate change impact studies, at least for near-term regional projections (Giuntoli et al. 2018). Hydrological simulations in natural ecosystems are always limited by simplified representation of complex processes occurring in the real world (Paturel et al. 2003; Clark et al. 2008; Dezetter et al. 2008). However, complex physically-based models do not necessarily yield better results than simpler models, especially in data-scarce regions, due to the large number of parameters and their inherent uncertainties (Singh and Marcy 2017). Identifying the most suitable hydrological model for a given purpose remains an outstanding challenge for the hydrological community. Nonetheless, a multi-model approach favouring different model structures provides better characterization of different hydrological processes (*e.g.* Clark et al. 2008, 2016). To address the caveat concerning hydrological model structures and bias correction methods, some researchers have suggested streamflow predictions using regression models based on large-scale climate teleconnections (*e.g.* Chiew and McMahon 2002; Kingston et al. 2013). As reported in Sidibe et al. (2019), most of these studies focus on specific regions (mainly regions with sufficiently long and complete observation records) and climatic indices, and therefore lack of reproducibility at larger spatial scales.

The comprehensive review of previous studies investigating the impact of climate change on water resources in West Africa by Roudier et al. (2014), underlines the fact that existing studies mainly focus on individual basins with climate change scenarios often provided by coarse spatial scale GCMs or early versions of RCMs. At the sub-continental scale, the impacts of climate change on hydrological systems over West and Central Africa are not fully understood (Washington et al. 2013; Roudier et al. 2014). The study by Stanzel et al. (2018) bridges this gap over West Africa by applying a multi-model ensemble of 15 RCMs from the CORDEX initiative (Coordinated Regional Climate Downscaling Experiment; Giorgi *et al.* 2009). However, in the latter, streamflow is estimated using a water balance model (at the annual timescale), which does not fully describe the complexity of hydrological processes. Moreover, climate projections are corrected using the widely applied delta-change approach, which, while stable and robust, does not account for potential future changes in climate decadal to multi-decadal variability and makes no distinction between extreme and normal events (i.e. the amount of change is similar for heavy rainfall and drizzle; Teutschbein and Seibert 2012).

Here, we aim to provide further insights into the response of hydrological systems to a changing climate across West and Central Africa by the mid-21st century. For this timeframe, climate projections are less sensitive to emission scenarios (*e.g.* Hawkins and Sutton 2009; IPCC 2013; Sylla et al. 2016), therefore, for simplicity, only results corresponding to a mitigation scenario (RCP4.5) are discussed in this paper. Climate simulations from the Rossby Centre Regional Climate model (RCA4) driven by nine

GCMs available within the CORDEX initiative are evaluated and bias-corrected using a nonparametric trend preserving quantile mapping approach (QDM; Cannon et al. 2015). We then use two conceptual hydrological models to understand hydrological processes at the subcontinental scale and provide future hydrological scenarios. For the first time, we also assess uncertainty in the traditional hydrological climate change impact modelling chain, through the implementation of a regression-based model linking streamflow with sea surface temperature (SST).

2. Data and Methods

The study area covers West and Central Africa (from 10°S to 25°N and 20°W to 30°E), with different climatic conditions: from arid in the northern fringe to tropical humid in the South. Hydrological regimes are described in Sidibe et al. (2018). Over the study area, 131 catchments with sizes ranging from 197 to 3,700,000 km^2 (median of 20,492 km^2) were considered.

2.1. Data

Streamflow and catchment properties (*e.g.* area, elevation, shape) datasets were collected from the SIEREM ("*Système d'Informations Environnementales sur les Ressources en Eaux et leur Modélisation*") database (Boyer et al. 2006; Dieulin et al. 2019). Over the study area, 131 discharge stations from the reconstructed streamflow dataset presented in Sidibe et al. (2018) were selected. Information about selected watersheds is provided in Appendix A.

Observed mean monthly precipitation (P), minimum and maximum temperature (T_{min} and T_{max}, respectively) datasets for the historical period (1951-2005) were collected from the Climatic Research Unit (CRU TS v4.00; Harris et al. 2014). Harris et al. (2014) found good agreement between the CRU dataset and other datasets, such as the Global Precipitation Climatology Centre (GPCC; Schneider et al. 2011). Due to the large scale of the study and climatic data availability/quality, evapotranspiration is estimated using relatively few input variables. The method used herein (eq. 1), after Droogers and Allen (2002), is a modified version of the Hargreaves approach (Hargreaves and Samani 1985), which accounts for precipitation as a proxy for insolation and relative levels of humidity. In data scarce environments, such an approach is a good alternative to the more physically based Penman-Monteith equation, which requires more input data (Allen et al. 1998). Mean external radiation is approximated from the latitude and the month of the year, after Allen et al. (1994).

$$ET0 = 0.0013 * 0.408Ret * (Tavg + 17.0) * (Td - 0.0123P)^{0.76} \qquad \textbf{(eq.1)}$$

With *P* the monthly precipitation amount (mm), R_{et} the extra-terrestrial radiation (MJ.m^{-2}), T_{avg} the average temperature (°C) and T_d the temperature range (°C).

The Extended Reconstructed SST version 5 (ERSST.v5, Huang et al. 2017) is used to develop multi-timescale linear regression models based on large-scale climate teleconnections. ERSST.v5 is a global monthly 2°×2° gridded SST dataset derived from the International Comprehensive Ocean–Atmosphere Dataset (ICOADS) Release 3.0. In addition, climate simulations (P, T_{max}, T_{min}) from nine GCMs of the fifth phase of the Coupled Model Intercomparison Project (CMIP5; Taylor et al. 2012), dynamically downscaled by the latest version of the Rossby Centre Regional Climate Model (RCA4), developed by the Swedish Meteorological and Hydrological Institute (SMHI) and available within the CORDEX framework, were collected via the Earth System Grid Federation (ESGF) data portals (Table 1).

Table 1: List of datasets and climatic variables used in the study

		Institution	Name	Variable	Period
Obs.		SIEREM, *France*	SIEREM	*Q, Area*	1951-2005
		CRU, *UK*	CRU TS v.4.00	*P*, T_{max}, T_{min}	1951-2005
		NOAA-NCDC, *USA*	ERSST.v5	*sst*	1951-2005
CMIP5 Mo	GCM	CCCma, *Canada*	CanESM2	*sst*	1951-2050

		CNRM, *France*	CNRM-CM5		
		CSIRO-QCCCE, *Australia*	CSIRO-Mk3-6-0		
		MOHC, *UK*	HadGEM2-ES		
		IPSL, *France*	IPSL-CM5A-MR		
		MIROC, *Japan*	MIROC5		
		MPI-M, *Germany*	MPI-ESM-LR		
		NCC, *Norway*	NorESM1-M		
		NOAA-GFDL, *USA*	GFDL-ESM2M		
	RCM	SMHI, *Sweden*	CanESM2_SMHI-RCA4	*P, Tmax, Tmin*	
			CNRM-CM5_SMHI-RCA4		
			CSIRO-Mk3-6-0_SMHI-RCA4		
			HadGEM2-ES_SMHI-RCA4		
			IPSL-CM5A-MR_SMHI-RCA4		
			MIROC5_SMHI-RCA4		
			MPI-ESM-LR_SMHI-RCA4		
			NorESM1-M_SMHI-RCA4		
			GFDL-ESM2M_SMHI-RCA4		

The multi-model ensemble is downscaled using a single RCM to constrain the uncertainty inherent to process representation within different RCMs, while RCM performances mainly relate to the quality of the GCM boundary forcing over West Africa (Kebe et al. 2016). Previous studies highlighted that the SMHI-RCA models satisfactorily represent different characteristics of historical precipitation and temperatures over West Africa (Nikulin et al. 2012; Mascaro et al. 2015; Stanzel et al. 2018).

Streamflow near-term projections (2020-2050) are then derived from two hydrological models, and a teleconnection-based regression model using SST fields from the nine aforementioned GCMs.

Due to the similarity in climate model responses to RCP forcing scenarios, over the near-term future (Hawkins and Sutton 2009; IPCC 2013; Aloysius et al. 2016; Sylla et al. 2016), we only present results for a mitigation scenario, *i.e.* RCP 4.5 (corresponding to a medium range emission and high mitigation with radiative forcings stabilized at 4.5 $W.m^{-2}$ and 650 ppm CO2 equivalent in the year 2100; Moss et al. 2010).

2.2. Methods

2.2.1. Bias correction

Climate simulations are compared to corresponding observed fields for the period 1951-2005 with Quantile Delta Mapping (QDM; Cannon et al. 2015) applied as a bias correction algorithm. Standard quantile mapping techniques are limited by the assumption of bias stationarity (*i.e. bias remains constant over historical and future periods*; Cannon et al. 2015). More advanced algorithms tackle this issue by applying quantile mapping on detrended time series (*i.e.* removing trend in the long-term mean) and reintroducing the trend afterwards (detrended quantile mapping). This however preserves only the climate change signal in the mean, while changes in other quantiles (extremes) are not accounted for. QDM preserves changes in simulated quantiles from climate models.

Discrepancies between model simulations and observations over a given period are corrected by: (1) detrending model-projected future quantiles and applying quantile mapping on the detrended series; (2) reintroducing projected trends on bias-corrected results, so that part of the climate sensitivity is preserved. More details about the different steps are provided in Cannon et al. (2015).

The method is applied at each grid point within the study area, and to each month individually for a better representation of seasonal cycles. Biases in future simulations (2006-2050) are corrected using transfer functions derived over the entire historical period (1951-2005) to mitigate to some extent the so-called “variability related apparent bias changes” (Maraun 2012).

A K-fold (K=11) cross-validation approach (Geisser 1975) is separately implemented to assess the performance of bias correction algorithms. For each grid-point, we generate a cross-validated time series consisting of all validation segments. Using these cross-validated timeseries, performance of the bias correction algorithms is first assessed with respect to the overall deviation between simulations and observations using the percent bias (PBIAS). Second, biases in cumulative distribution functions (CDFs) are also investigated using the Kolmogorov-Smirnov (K-S) test, with the null hypothesis being that both samples (observations and simulations) are drawn from the same statistical distribution and the K-S test statistic D, the maximum difference between CDFs.

2.2.2. Hydrological modelling

Identifying the most appropriate model structure for the characterization of hydrological processes and quantifying associated uncertainties are the main challenges facing the hydrological community (Clark et al. 2008). In this study, two hydrological models (GR2M and IHACRES) are used to investigate the impacts of climate change on streamflow over West and Central Africa. Both models are computationally attractive (due to few calibration parameters), and therefore convenient for data-scarce environments.

GR2M is a two parameter spatially lumped conceptual monthly rainfall-runoff model developed by IRSTEA (*Institut national de recherche en sciences et technologies pour l´environnement et l´agriculture*). In the version used herein (developed by Mouelhi et al. 2006), hydrological processes are described using two reservoirs: a production reservoir with capacity X1 and a routing reservoir (fixed capacity of 60 mm), whose interactions with groundwater systems are governed by the parameter X2 (Figure 1a). Due to its robustness and very low input data requirement (precipitation, potential evapotranspiration and streamflow), the GR2M model has been extensively used in West and Central Africa (*e.g.* Paturel et al. 1995; Ardoin-Bardin et al. 2009; Ibrahim et al. 2015).

The IHACRES model is a conceptual-metric model built upon a non-linear soil moisture accounting module (Jakeman et al. 1990), which converts total precipitation into effective rainfall and a linear routing module generating stream discharge from effective rainfall. In this study, the model is implemented at monthly time steps and the non-linear soil moisture accounting module is based on the Catchment Wetness Index (CWI; Jakeman and Hornberger 1993), where effective rainfall is proportional to an antecedent soil moisture index and a scaling factor used to enforce mass balance. The soil moisture accounting module is built upon three main calibration parameters: the drying rate at reference temperature, the temperature dependence of drying rate and the mass balance term. The linear routing module is represented by two reservoirs (quick flow and baseflow) in parallel. The outflow is then processed using ARMAX-type (auto-regressive moving average with exogenous inputs) linear transfer functions (Jakeman et al. 1990) to generate simulated streamflow (Figure 1b).

Such a formulation reduces parameter uncertainty inherent to hydrological models, while at the same time attempting to characterize internal hydrological processes (Croke and Jakeman 2004). This model implemented for the Niger River basin by Oyerinde et al. (2016) yielded satisfactory results.

2.2.3. Regression-based SST-streamflow model

Sidibe et al. (2019) found streamflow variability in West and Central Africa to be significantly associated with SST anomalies in the Pacific and Atlantic Oceans at different timescales: interannual (~2-5 years) to multi-decadal (> 20 years). Such relationships are similar to those detected for rainfall over the region (*e.g.* Mohino et al. 2011; Rodriguez-Fonseca et al. 2015; Dieppois et al. 2013, 2015). Building upon these teleconnections, we thus use multiple regressions of annual streamflow on empirical orthogonal functions (EOFs) of SST fields following the modelling strategy developed by Benestad (2001). This approach is modified based on Massei et al. (2017) findings, who integrated a discrete wavelet multiresolution analysis, to capture the main modes of variability, *i.e.* predictors, at different timescales.

In data-scarce regions, due to the lower number of input variables (streamflow and SSTs), this streamflow prediction strategy could potentially help narrowing the uncertainty associated with the quality of gridded observational datasets (e.g. rainfall and temperature), built upon spatio-temporal interpolation techniques, which impact hydrological model performances, climate model evaluation and bias-correction algorithms, resulting in misleading streamflow projections. The main steps are: (1) to generate individual predictor datasets (1951-2050) by combining (along the time axis) observations (ERSST v5) and GCMs SST fields; (2) to extract wavelet details using the Maximum Overlap Discrete Wavelet Transform (MODWT; Percival and Walden, 2000) for both predictors and predictands; (3) to implement one regression model for each wavelet decomposition level of the atmospheric field and local hydrometeorological variables using the common EOF analysis; and (4) to reconstruct the final time series by summing up all models at the end of the process.

Principal components (PCs) of the 20 leading EOFs, which represent the observation part of the combined dataset, are used as predictors to develop linear step-wise regression models. The selected PCs derived from future GCM simulations are then used to generate streamflow projections. Using the common EOF analysis ensures the physical consistency of climate model simulations (Benestad 2001).

A K-fold cross-validation is also implemented (K=11), and performance is assessed with the Kling Gupta efficiency criteria (Kling et al. 2012).

3. Climate scenarios: evaluation and bias correction

3.1. Model evaluation

Rigorous regional-scale evaluation of climatic variables´ seasonal cycles is of paramount importance for impact studies (Eyring et al. 2019). The ability of climate models to reproduce historical (1951-2005) climatic patterns is assessed relatively to the CRU observation datasets.

3.1.1. Precipitation patterns

The spatial distribution of precipitation (long-term means) for the period 1951-2005, is characterized by a strong meridional gradient, with highest amounts found in the Southwest and Southeast of West Africa and Central Equatorial Africa (Figure 2a), as observed by Mahé et al. (2001). Major parts of the study area receive around 60 mm.month^{-1}, with maximum reaching 253 mm.month^{-1} (Figure 2a). Most models are able to capture this meridional gradient, but dissimilarities are observed in the representation of the spatial extent and rainfall amounts (figure 2b). Over West Africa, most models except CNRM and CSIRO capture relatively well the regions of maximum precipitation, despite overestimations along the Guinean highlands (Figure S1), as suggested by Akinsanola et al. (2018). In addition, precipitation patterns over the Sahel (between 11°N and 18°N) are generally well-represented, except for CanESM2 and IPSL, where the region of minimum rainfall (<25 mm.month^{-1}) extends southwards to 15°N. This can be attributed to model representation of the ITCZ northward propagation and gradual southward retreat (Nikulin et al. 2012). In fact, all models fail at representing the pattern observed in Central Equatorial Africa (Figure 2a-b), leading to higher biases in total precipitation. More specifically, the magnitude of deviation between RCA4 simulations and CRU observations (assessed using the PBIAS) over the entire historical period (1951-2005) underlines a dry bias (between -20% and -35%) in Central Africa regardless of the driving GCMs (Figure 2c-k), consistently with the findings of Aloysius et al. (2016). A dry bias is also observed in the Guinean

Coastal regions (4°N-8°N) for most models, except MIROC5 (median PBIAS of +6.4%) (Figure 2c-k). Further North, the influence of driving GCMs becomes more important. In Sudanian (8°N-11°N) and Sahelian (11°N-18°N) regions for instance, models such as CanESM2, CNRM, HadGEM2, IPSL and NCC present negative biases (reaching -62.9% for IPSL), while others present wet biases (up to +40% for CSIRO over the Sahel). Overall the mean climatology is best represented by HadGEM2, MIROC5, GFDL and MPI (Figure 2f, h, i, k). Similar results are found for the NRMSE statistic (not shown).

The deviations between simulations and observations result in bias in the CDFs. As determined using the KS-test, most of the study area is characterized by high dissimilarity between statistical distributions of observations and simulations (Figure 3a). Highest differences (K-S test statistic $D > 0.5$) can be observed in Central Equatorial Africa (Figure 3a). At $p \leq 0.1$, multi-model agreement indicates that less than 5% of the study area presents significantly similar statistical distributions (Figure 3b). The dissimilarity is however smaller between 12°N and 18°N for most models (except CSIRO and IPSL), confirming a good representation of rainfall distributions over the Sahel (Figure 3a). For each model, the ability to reproduce the seasonal cycle is also investigated (cf. Figure S2). For all models, the critical value ($D = 0.1645$) at $p \leq 0.1$ is in general exceeded for each month. The lowest values are observed between December and February, albeit with the highest inter-quartile range (Figure S2). Highest dissimilarities occur from May to October (Figure S2), suggesting that uncertainties mainly arise from the representation of the West African Monsoon (WAM) meridional migrations, as described by Sultan and Janicot (2000).

3.1.2. Minimum and Maximum temperatures

Similar to long-term precipitation, maximum temperatures over the study area are characterized by a strong meridional gradient with highest temperatures reported along the Sahelian band (>35°C) and lowest maximum temperatures in western Central Africa (20-25°C) (Figure 4a). This meridional pattern is relatively well represented by most models, except CNRM, CSIRO and GFDL (not shown). The median absolute bias over the study area suggests that majority of the models present a cold bias ranging from -0.37°C in HadGEM2 to -1.30°C in GFDL (Figure 4c-k). This cold bias is predominantly located in Sudanian and Sahelian regions (Figure 4c-k), as already reported by Sarr (2017). From the Gulf of Guinea to Central Africa, most models present warm biases, ranging from +0.84°C in GFDL to +2.7°C in IPSL.

For minimum temperatures, the long-term climatology highlights a zonal gradient, where most of West Africa (up to 21°N) is warmer (20°C-25°C) than eastern and Central Africa (15°C-20°C; Figure 5a). This zonal pattern is best reproduced by CSIRO (median absolute bias -0.13°C), MIROC5 (median absolute bias of -0.17°C) and IPSL (median absolute bias of 0.18°C), showing the lowest biases over the region (Figure 5e, h, g). All models are characterized by a cold bias ranging from -0.74°C in MIROC5 to -3.18°C in CNRM (Figure 5c-k), which similarly to maximum temperatures is located along the Sahelian band (Figure 4c-k). Moreover, the amplitude of the warm bias detected for maximum temperatures over the Gulf of Guinea and Central Africa is dampened: from +0.42°C in MIROC5 to +1.68°C in IPSL (Figure 5h, g).

Biases in CDFs are also found in historical simulations for temperature, with the highest K-S test statistic D observed in Central Equatorial Africa (Figure 6a, c). We note that distributional biases in minimum temperatures are higher than those observed for maximum temperatures (Figure 6c). In addition, multi-model agreement highlights that less than 2% of the study region present significantly similar CDFs at p ≤ 0.1 (Figure 6b, d).

Seasonal cycles of distributional biases in T_{max} and T_{min} underline high discrepancies (median K-S test statistic D ranging from 0.4 and 0.8; Figure S3-4). While distributional biases in maximum temperature are more important between May and October (Figure S3), those observed in minimum temperature are homogenous throughout the year with no marked seasonality (cf. Figure S4).

According to Sarr (2017), the predominant cold bias observed for the different temperature fields over the study area is mainly due to the misrepresentation of climatic processes in GCMs. Other factors, such as excess cloudiness, surface albedo, and aerosols could play an important role (*e.g.* Giannini et al. 2003; Nicholson 2013).

3.2. Bias correction and cross-validation

Model evaluation highlighted important biases in precipitation and temperatures. The bias correction algorithms were thus applied to all hydroclimatic variables. For application in hydrological climate change impact studies, it is crucial that biases are also corrected in the seasonal cycle.

Cross-validation results highlight the ability of the QDM algorithms to satisfactorily reduce these biases (Figure 7). In fact, median PBIAS over the study area is now within the range ±1.1% for precipitation fields (not shown). More importantly, higher order moments are also improved in precipitation: median ratio of standard deviations derived from bias-corrected and raw data over the study area is around 1.05 for all models (not shown). In precipitation, the distributional biases are thus significantly reduced for more than 55% of the study area (Figure 7a-c). Distributional biases in the seasonal cycle are also significantly corrected with median K-S test statistic D below 0.2 at $p \leq 0.1$ (cf. Figure S2).

In general, bias correction algorithms yielded better results for temperatures compared to precipitation, with median absolute bias of ±0.05°C (standard deviation ratio of 1.02; Figure 7d-i).

In maximum temperatures, distributional biases are corrected (at $p \leq 0.1$) for more than 80% of the study area (Figure 7d-f). Significant biases however remain over parts of Central Africa, where multi-model agreement is low (Figure 7e).

Similar patterns are identified for minimum temperatures (Figure 7g-i), with however residual significant distributional biases extending to the Gulf of Guinea coastal regions (Figure 7h). Seasonal distributional dissimilarities in maximum and minimum temperature are also satisfactorily corrected (cf. Figure S3-4).

Despite overall good performances, the bias correction algorithms presented limited skill in Central Equatorial Africa, where distributional biases remain significant. This can be attributed partly to the lack of observed gauge data over the region (New et al. 2000; Nikulin et al. 2012), resulting in a limited representation of the regional climatic processes, and therefore difficulties in model evaluation and bias correction. In addition, several GCMs present the so-called “double ITCZ problem” (Lin, 2007), characterized by precipitation overestimation off the equator, and underestimation along the equator, over Central Africa, as a result of poor representation of climate processes controlling the formation and propagation of Mesoscale Convective Systems (MCSs) (Aloysius et al. 2016). Disentangling the part of uncertainties related to the quality of observation gridded-data and to climate models is however difficult. Further details about model parametrization, performances and potential inadequacies in tropical regions are provided in Monerie et al. (2012), Washington et al. (2013) among others.

4. Hydrological modelling: calibration and validation

According to Sidibe et al. (2018), missing information in discharge time series over the region mainly occur in the early 1950s and 2000s. To reduce the uncertainty associated with the reconstructed streamflow datasets, the 1960-1999 period has thus been selected to quantify hydrological model parameters. Models are calibrated using automated calibration algorithms on a decade and validated on the next, with a warm-up period of 5 years, before each calibration interval. Calibration intervals are also used for validation to assess model robustness. Two different performance criteria are used to assess model efficiency: the Nash-Sutcliffe efficiency criterion (NSE; Nash and Sutcliffe 1970) and the modified Kling-Gupta criterion (Kling et al. 2012). Both models are calibrated through sampling the parameter space: uniform grid screening for GR2M (Michel 1991) and Latin hypercube sampling (LHS; McKay et al. 1979) for IHACRES-CWI.

Even though simple in their parametrization, the hydrological models were able to capture to some extent the complexity of hydrological processes occurring over the study area. Both models perform well over most of the region, with median KGE higher than 0.7 (median NSE above 0.75) (Figure S5). GR2M however, seems to perform slightly better than IHACRES-CWI, which present higher inter-quartile ranges. For GR2M, we also note that performances tend to be better when models are calibrated on relatively drier periods (*i.e.* 1970s and 1980s), as suggested by Dezetter et al. (2008) for 49 river basins over the same region.

Despite overall good performances, the implemented hydrological models showed limited skill locally. For instance, GR2M performs poorly (KGE < 0.4) over the Niger

River middle reach (*e.g.* at Tossaye [MLQ0036] and Niamey [NEQ2000]; Figure 8). This may be due to the impact of the Inner Niger Delta (flooded area ~40,000 km2 resulting in annual water losses of ~40%), which significantly modifies downstream rainfall-runoff relationships (Mahé et al. 2009; Zaré et al. 2017). Low performances are also observed in GR2M for basins in the northeastern part of the study region (*e.g.* at Logone Gana [TDQ5006]) and the northern fringe of the Congo basin (*e.g.* at M'bata [CFQ0034], Bwembe [CGQ0013] and Gamboma [CGQ0017]; Figure 8a, b). This could be explained through changes in runoff coefficients after 1970, due to changes in land use and persistent degradation of the woody cover in the Sahel, as described by Mahé et al. (2005) and Mahé and Paturel (2009), and/or to the quality of gridded observational data over Central Africa, where few stations were assimilated to build the CRU dataset (New et al. 2000; Nikulin et al. 2012; Aloysius et al. 2016).

Interestingly, we note that IHACRES-CWI capture to some extent the hydrological conditions downstream the Inner Niger Delta (Figure 8c, d). This results from the linear routing function, which accounts for a lag-time between input and simulated outflow. However, this model presents limited skill in parts of Central Africa (*e.g.* at Bwembe [CGQ0013] and Gamboma [CGQ0017]), and over humid regions of West Africa (*e.g.* Hetin Sota [BJQ0036]), where Mahé et al. (2005) found significant changes in groundwater levels. This might thus highlight limitations in IHACRES-CWI, which does not account for groundwater interactions.

As illustrated in Figure S6, model parameters could slightly change from one period to another due to climate variability (*e.g.* changes in frequency and intensity of rain events) and/or changes in land use (Niel et al. 2003; Dezetter et al. 2008; Ibrahim et al. 2015). To better account for non-stationarity in model parametrization, future streamflow scenarios presented in Section 3.4.3 were thus derived using model parameters estimated for the 1970-1999 period, which roughly corresponds to an average response of the system (Figure S6).

5. Linear regression-based streamflow SST model

Previous studies seeking to link local climatic variables with large-scale SST anomalies indicated the importance of predictor domain size on linear model skill (*e.g.* Benestad 2002; Mtongori et al. 2016). In this study, we found that a domain comprising the Atlantic and Pacific basins results in higher cross-validation performances (median KGE ~ 0.4). The spatial distribution of model efficiency highlights good skill for most catchments (Figure 9). However, the results contrast slightly with the hydrological models presented in the previous sections. In fact, poor performances (KGE < 0.4) are now mainly observed on the upper Niger River reach, *i.e.* from the Guinean highlands to southern Mali (Figure 9). Similar results also are observed in parts of the Volta basin and in some regions of northern and western Central Africa (Gabon; Figure 9). These results might stem from weak predictor-predictand relationships and human-induced catchment modifications. Interestingly, we observe that some catchments in Central Africa, where hydrological models were performing poorly now present better results (see Appendix A). For instance, over parts of Central Africa (e.g. the N'Keni basin at Gamboma [CGQ0017]), the regression model outperformed (KGE > 0.8) the hydrological models (KGE < 0.2), which were mainly impacted by the quality of observed gridded precipitation and temperature datasets. This highlights the potential added-value of teleconnections-based regression models in data-scarce environments, where gridded observational datasets quality is likely to be poor, for improved predictions.

6. Future hydroclimatic variability in West and Central Africa by mid-21st century

6.1. Changes in near-term precipitation

In Figure 10, near-term (2020-2050) projected precipitation changes relative to the historical period are explored under the RCP4.5 emission scenario. Most models (except CSIRO [-2.2%] and MPI [-2.1%]) show slight positive relative changes over the study area (from 2 to 12%; Figure 10). Good agreement is observed between uncorrected simulations and bias-corrected data (not shown).

In Central Africa, the mid-21st century will be characterized by slight changes (±4%) with a trend towards wetter conditions, within the range predicted by Aloysius et al. (2016) using the same emission scenario. A similar pattern is identified along the Gulf of Guinea coastal regions, where GFDL and MIROC5 both predict higher relative changes in precipitation of around +8.5% and +6.7%, respectively (Figure 10i, f). Further North, along the Sahelian strip, relative changes are more significant, with highest changes predicted by CanESM2 (+17%), MIROC5 (+16.4%), NCC (+15.8%) and HadGEM2 (+12%).

In addition, the Sahelian band presents a zonal contrast, with its westernmost part drier than central and eastern regions (except for CNRM, MIROC5, NCC and GFDL). This pattern is consistent with previous investigation of future rainfall in the Sahel (*e.g.* Monerie et al. 2012; Sylla et al. 2016). Over the westernmost part of the Sahel, precipitation decrease of up to -22% is reported in IPSL (Figure 10e). In the central and eastern regions, most models (except CSIRO, MPI and GFDL) predict significant positive changes: CanESM2 (+28%), NCC (+28%), MIROC5 (+23%), HadGEM2 (+18.6%) IPSL (+16%) and CNRM (+8.7%).

6.2. Changes in near-term temperatures

Absolute changes in temperature by the mid-21st century over West and Central Africa show significant warming trends, with an overall good agreement between models (Figure 11).

Changes in maximum temperatures are expected to range between +1.2°C and +1.9°C (Figure 11). Spatial patterns, however, suggest regional contrasts (Figure 11). For instance, greater warming tends to be observed in Central Africa and over the northern fringe (Sahara) of the study area, while weaker warming tends to be identified along the Gulf of Guinea coastal regions (Figure 11).

According to Figure 12, over the study area minimum temperatures rise faster than maximum temperatures by the mid-21st century, consistently with previous findings (Funk et al. 2012; Ringard et al. 2016; Sarr 2017). Median warming anomalies range between +1.4°C in CNRM and +2.2°C in IPSL (Figure 12b, e). By the mid-21st century, all models, but one (CNRM), predict minimum temperatures anomalies larger than +1.7°C.

Temperature trends presented in this study corroborate previous findings describing Sahelian and tropical West African regions as hotspots of climate change (IPCC 2014; Niang et al. 2014; Sylla et al. 2016).

6.3. Discharge evolution by the mid-21st century in West and Central Africa

Changes in river discharge are explored relatively to the historical period using two conceptual hydrological models in Figure 13-14, and a multi-timescale regression-based model in Figure 15. Projections are compared to historical streamflow generated with calibrated model parameters and bias-corrected hydroclimatic variables rather than observed streamflow to limit the uncertainty related to residual biases in the mean of bias-corrected climate inputs.

With respect to the long-term historical percent bias presented in Section 3.1.1, models such as HadGEM2, MIROC5, GFDL and MPI (see Figure 2f,h, i, k) provided good representation of precipitation patterns (long-term means), indicating quality of model simulations and good representation of climate processes (Eyring et al. 2019). If these models are likely to provide robust streamflow projections with limited impact of bias-correction uncertainties, at the regional scale, others such as IPSL, CanESM2 and CSIRO (high biases over the Sahel and Sudanian regions; Figure 2g, c, e) might result in uncertain streamflow projections.

Despite differences in their ability to capture some hydrological processes, hydrological models generally predicted consistent changes in streamflow over the region and show slight changes in river discharge by the mid-21st century. Uncertainties appear to result mainly from climate model projections. Depending on the driving GCMs, we observe differences in the proportion of area with significant streamflow changes at $p \leq 0.1$: CanESM2 (38.2%), CNRM (20%), CSIRO (36%), HadGEM2 (33.6%), IPSL (14.5%), MIROC5 (59.5%), MPI (10%), NCC (36.6%) and GFDL (42.7%).

Using the GR2M model, projected climate variables result in positive streamflow changes ranging from +1.4% to +19.4% on average across the study region (Figure 13) for all models, except CSIRO (-9.4%), which presented important biases in historical precipitation. More specifically, most parts of Central Africa, where GR2M presented limited skill and climate model evaluation indicated important dry and warm biases, present slight uncertain changes ±5% (with most models predicting wetter conditions; Figure 13). Along the Gulf of Guinea up to 11°N, where hydrological regimes are bimodal (Descroix et al. 2009; Roudier et al. 2014), changes are mostly positive, reaching +23.5% in MIROC5 (Figure 13). Changes in the Gambia River basin are uncertain, with some models predicting negative changes mainly in the headwater (CNRM, CSIRO, IPSL, MIROC5 and MPI), and others slightly positive changes (CanESM2, HadGEM2, NCC and GFDL). Further North, in the Sahelian regions, where GR2M presented good skill (except the Inner Niger delta region) and climate models showed a predominant cold bias, changes in river discharge are even stronger (Figure 13). Over this region, which comprises the Senegal and the upper reach of the Niger River, the highest relative changes in streamflow are predicted by HadGEM2 (+22.5%), MIROC5 (+21%), CanESM2 (+18.7%) and NCC (+18.4%). Although positive trends in river discharge are consistent with predicted rainfall, they could appear counterintuitive considering the expected increase in temperatures and evapotranspiration. This is nonetheless consistent with a recent assessment of future water availability by Sylla et al. (2018), suggesting that increased precipitation overcompensates the increased evapotranspiration.

In general, similar patterns are observed using IHACRES-CWI model (Figure 14). Except CSIRO and IPSL which show negative changes in river discharge, West Africa is mostly characterized by positive trends using IHACRES-CWI (Figure 14), consistently with GR2M predictions. Median changes over the study area are also relatively smaller in IHACRES-CWI compared to GR2M which tends to be wetter (Figure S7). This is probably inherent to the structure of IHACRES-CWI, which accounts for catchment moisture levels. In Central Africa, projected changes are uncertain with most models predicting relatively small positive changes ranging from +0.1% to +6.8%, while the rest of the models present negative changes ranging from -5% to -8% (CanESM2, CSIRO, IPSL; Figure 14). At the regional scale, the fact that negative changes are predicted by models which presented important biases in historical precipitation (CSIRO, CanESM2 and IPSL), indicating limitations in the representation of climate processes, provides more confidence in wetter conditions. In addition, at the catchment scale, we note positive changes for catchments in the Gulf of Guinea region (*e.g.* Sassandra [+11%], Bandama [+11%]), except for the Cavally basin, where changes are of opposite signs for GR2M (+5%) and IHACRES-CWI (-1.2%). Even though streamflow projections are consistent across the study area for both hydrological models, results should be interpreted with caution, particularly over Central Africa and parts of the Gulf of Guinea, where uncertainty remains high regardless of the driving GCM, as indicated by bias-correction results (cf. Section 3.2). Using the multi-timescale regression-based model, discharges in West and Central Africa by the mid-21st also present slight positive changes (from +2% to +27%) for most models (Figure 15), except in CNRM (-1.1%), CSIRO (-20%) and MPI (-15%), at the regional scale. In Central Africa, in particular, where the linear-regression model presents sometimes higher prediction skill compared to hydrological models, streamflow changes range from -8% (NCC) to +2.5% (GFDL) and can even reach +15% using HadGEM2 (Figure 15). Over the Gulf of Guinea and Sudano-sahelian regions, predicted changes are more important, yet more uncertain. In these regions, most models present changes in the range of +5%, approximately, and +25% using HadGEM2 (Figure 15d). Reversely, negative changes are found using CSIRO, and reach up to -40% using MPI (Figure 15c, g). Median changes in streamflow over the study area are summarized in Figure S8. In addition, at the catchment scale, the Bandama catchment shows contrasting results for the linear regression model regardless of the driving GCM (median change ~ -12%). This could have resulted from complex predictor-predictand relationships, which are not fully captured by the regression-based model.

These results suggest that for some regions in Central Africa, where strong SST-streamflow teleconnections exist, regression models can serve as an alternative to hydrological models that require more input data. However, the higher spread of predictions observed over the Gulf of Guinea and Sudano-sahelian regions underline the need for larger multi-model ensembles for a better representation of predictor (SST) fields. In their evaluation of SST patterns from CMIP5 models (22 models), Wang et al. (2014) highlighted important biases (too low values in the Northern Hemisphere and too high values in the Southern Hemisphere) mainly resulting from model misrepresentation of physical processes and feedback mechanisms. For example, the amplitude of Global SST biases is significantly associated with model capacity to characterize the Atlantic Meridional Overturning Circulation (AMOC): biases increase as the AMOC circulation weakens. Findings also highlighted important biases in the representation of decadal modes of global SST variability and El-Nino-Southern Oscillation (ENSO) patterns. These discrepancies in climate models representation of ENSO, which result from overestimations over the western regions and underestimations over the eastern regions, are particularly important in CSIRO and IPSL (which fail at capturing the seasonality of ENSO) and less pronounced for models such as MIROC5 and CNRM (Dieppois et al. 2015, 2019). For improved projections, climate models which present less bias in the representation of key SST patterns and their modes of variability should be preferred (*e.g.* MIROC5, CNRM).

Although based on a single RCM, the findings presented in this section are consistent with previous investigation of near-term river flow evolution in West Africa under similar emission scenario (Ardoin-Bardin et al. 2009; Roudier et al. 2014; Aich et al. 2014; Mbaye et al. 2015; Yira et al. 2017; Stanzel et al. 2018), except for the Gambia River basin where most studies predict significant negative trends. For instance, Bodian et al. (2018) found a decrease of up to -22% for the near-term future using a set of six GCMs (statistically downscaled with the delta change method) and the GR4J hydrological model. However, different results could have resulted from the use of the RCA4-RCM, which has a tendency towards wetter projections over West Africa compared to other RCMs (Stanzel et al. 2018).

7. CONCLUSIONS

In this study, we investigated the impact of near-term (2020-2050) climate variability and change on hydrological systems over West and Central Africa using a regional multi-model ensemble, bias correction algorithms and different runoff modelling strategies.

Evaluation of climate model outputs, performed to quantify biases and therefore help assess performance of bias-corrections techniques, highlighted different levels of accuracy in the representation of key WAM features, resulting in important dissimilarities. For instance, biases in precipitation are often associated with model representation of the ITCZ intensity and northward propagation (Nikulin et al. 2012). Over Central Equatorial Africa, however, these biases were more important regardless of the driving GCMs. This can be attributed to the quality of gridded observational datasets over this region and other factors such as representation of topography and climate processes controlling the formation and propagation of MCSs (Aloysius et al. 2016).

Two different approaches were adopted to assess future changes in streamflow over the region. Firstly, bias correction algorithms were applied to climatic variables (precipitation, maximum and minimum temperatures) prior to their use in two conceptual hydrological models. These bias correction algorithms satisfactorily reduced discrepancies between model simulations and observations, and importantly preserved the climate change signal predicted by climate models. However, the bias correction presented limited skill over Central Equatorial Africa, stemming mainly from the quality of observational stations (New et al. 2000; Nikulin et al. 2012) impacting gridded datasets. Input data quality in this region might have also impacted hydrological models, which performed poorly. Elsewhere, hydrological models presented higher skill, and more importantly, their different structures satisfactorily characterized different important hydrological processes: while GR2M provided insights for regions with important groundwater interactions, IHACRES-CWI satisfactorily captured complex hydrological processes occurring downstream the Inner Niger Delta and the Benue River.

Secondly, streamflow projections were derived based on large-scale SST teleconnections using multi-timescale linear regression models (Massei et al. 2017). This latter procedure, implemented here for the first time across West and Central Africa, appeared as an alternative to hydrological models for impact studies in data-scarce regions with robust streamflow-SST teleconnections. For instance, in parts of Central Africa (*e.g.* the N'Keni basin at Gamboma [CGQ0017]), the regression model outperformed (KGE > 0.8) the hydrological models (KGE < 0.2), which were mainly impacted by the quality of observation datasets. This regression model nevertheless presented limited skill over the upper reach of the Niger River in the Guinean and Sudanian regions, where complex SST teleconnections were highlighted in previous studies (Wotling et al. 1995; Nicholson 2008; Sidibe et al. 2019).

West and Central Africa are found to be characterized by slightly wetter conditions by the mid-21st century under RCP4.5 scenario, and, according to previous studies (Hawkins and Sutton 2009; IPCC 2013; Sylla et al. 2016), these results are expected to be similar to those of more optimistic or pessimistic scenarios (e.g. RCP2.6 and

8.5). In fact, similarities were detected in future precipitation over the region, with less than 4.5% of the study area presenting significant ($p \leq 0.1$) differences between RCP4.5 and 8.5 (not shown). Overall, precipitation is likely to increase within a range of +2 to +12%. Important spatial variability is however observed locally over Central Africa (±4%) and across the Sahel, where some models present a zonal contrast (up to -22% in the western part and up to 28% in the eastern part). Temperatures present a sustained increasing rate (higher for minimum temperatures) between +1.2°C and +2.2°C, with highest absolute changes occurring mainly along the Sahelian band.

These future trends in climatic variables are therefore likely to result in slight positive streamflow changes (~ +5%), which are consistent across the different modelling strategies, despite local differences. Importantly, these wetter conditions are predicted by climate models which presented reduced biases in historical precipitation, suggesting less influence of bias-correction uncertainties. The pattern closely mimics the change in rainfall, with smaller (higher) changes in Central Africa (further North). Despite agreements in streamflow projected change over the entire study area, a higher interquartile range (±40%) is observed for the linear regression-based model, due to uncertainties in SST simulations. This is especially true for the different future trajectories of main modes of variability in the Atlantic and Pacific Oceans (*e.g.* ENSO, AMO) predicted by CMIP5 models (*e.g.* Wang et al. 2014; Dieppois et al. 2019). Notwithstanding the uncertainties in streamflow projections over the study area, we showed here that reducing the steps in traditional hydrological climate change impact studies, can help improve predictions of changes in data-scarce regions. Nonetheless, further investigations with larger multi-model ensembles are required to shed the light on uncertainties associated with SST projections, streamflow large-scale climate teleconnections, and help assess the full spectrum of future streamflow fluctuations.

Recent developments in statistical post-processing of climate information (*e.g.* multi-variate bias-correction; Robin et al. 2019) might also help improve projection of changes.

In addition, river flow projections presented in this study account only for climate change and variability. It should not be forgotten that an expected population increase in Sub-Saharan Africa by 2050 (population expected to approach 2 billion people) will result in rising demand posing substantial threats to water security (quantity and quality; Serdeczny et al. 2017), and greatly modifying hydrological regimes (Mahé et al. 2013). Detailed investigations must be conducted to integrate the influence of three other key aspects significantly impacting river flow (Sterling et al. 2013): land use, water consumption/withdrawal and carbon effect on plant water use. This will require an integrated approach with different modelling strategies but most importantly a joint effort for data collection and sharing across key actors (*e.g.* national water offices, water practitioners, stakeholders) in sub-Saharan Africa.

Acknowledgements

Moussa gratefully acknowledges the funding received towards his PhD studies from Coventry University, UK, and resources provided by the Centre for Agroecology Water and Resilience (CAWR). The authors are also grateful to the developers and maintainers of R packages (**airGR, esd, Hydromad, MBC and wmtsa**) used in this study. Authors also thank the National hydrological services in Africa which collected discharges data used in this study.

References

Aich, V., Liersch, S., Vetter, T., Huang, S., Tecklenburg, J., Hoffmann, P., Koch, H., Fournet, S., Krysanova, V., Müller, E.N., Hattermann, F.F., 2014. Comparing impacts of climate change on streamflow in four large African river basins. Hydrol. Earth Syst. Sci. 18, 1305–1321. https://doi.org/10.5194/hess-18-1305-2014

Akinsanola, A.A., Ajayi, V.O., Adejare, A.T., Adeyeri, O.E., Gbode, I.E., Ogunjobi, K.O., Nikulin, G., Abolude, A.T., 2018. Evaluation of rainfall simulations over West Africa in dynamically downscaled CMIP5 global circulation models. Theor. Appl. Climatol. https://doi.org/10.1007/s00704-017-2087-8

Allen, R.G., Luis, S.P., RAES, D., Smith, M., 1998. FAO Irrigation and Drainage Paper No. 56. Crop Evapotranspiration (guidelines for computing crop water requirements). Irrig. Drain. https://doi.org/10.1016/j.eja.2010.12.001

Allen R. G., Smith M., Pereira L. S., Perrier A., 1994. An update for the calculation of reference ' evapotranspiration. ICID Bulletin of the International Commission on Irrigation and Drainage, 35–92.

Aloysius, N.R., Sheffield, J., Saiers, J.E., Li, H., Wood, E.F., 2016. Evaluation of historical and future simulations of precipitation and temperature in central Africa from CMIP5 climate models. J. Geophys. Res. https://doi.org/10.1002/2015JD023656

Ardoin-Bardin, S., Dezetter, A., Servat, E., Paturel, J.E., Mahé, G., Niel, H., Dieulin, C., 2009. Using general circulation model outputs to assess impacts of climate change on runoff for large hydrological catchments in West Africa. Hydrol. Sci. J. https://doi.org/10.1623/hysj.54.1.77

Benestad, R.E., 2002. Empirically downscaled multimodel ensemble temperature and precipitation scenarios for Norway. J. Clim. https://doi.org/10.1175/1520-0442(2002)015<3008:EDMETA>2.0.CO;2

Benestad, R.E., 2001. A comparison between two empirical downscaling strategies. Int. J. Climatol. https://doi.org/10.1002/joc.703

Bodian, A., Dezetter, A., Diop, L., Deme, A., Djaman, K., Diop, A., 2018. Future climate change impacts on streamflows of Two Main West Africa River Basins: Senegal and Gambia. Hydrology. https://doi.org/10.3390/hydrology5010021

Boyer, J.F., Dieulin, C., Rouche, N., Cres, A., Servat, E., Paturel, J.E., Mahé, G., 2006. SIEREM: An environmental information system for water resources, in: IAHS-AISH Publication.

Bürger, G., J. Schulla, and A. Werner, 2011: Estimates of future flow, including extremes, of the Columbia River headwaters. Water Resour. Res., 47, W10520. https://doi.org/10.1029/2010WR009716

Cannon, A. J., 2016. Multivariate bias correction of climate model output: Matching marginal distributions and intervariable dependence structure. *Journal of Climate*, *29*(19), 7045-7064.

Cannon, A.J., Sobie, S.R., Murdock, T.Q., 2015. Bias correction of GCM precipitation by quantile mapping: How well do methods preserve changes in quantiles and extremes? J. Clim. https://doi.org/10.1175/JCLI-D-14-00754.1

Chiew, F.H.S., McMahon, T.A., 2002. Global ENSO-streamflow teleconnection, streamflow forecasting and interannual variability. Hydrol. Sci. J. 47, 505–522. https://doi.org/10.1080/02626660209492950

Clark, M.P., Slater, A.G., Rupp, D.E., Woods, R.A., Vrugt, J.A., Gupta, H. V., Wagener, T., Hay, L.E., 2008. Framework for Understanding Structural Errors (FUSE): A modular framework to diagnose differences between hydrological models. Water Resour. Res. 44. https://doi.org/10.1029/2007WR006735

Clark, M.P., Wilby, R.L., Gutmann, E.D., Vano, J.A., Gangopadhyay, S., Wood, A.W., Fowler, H.J., Prudhomme, C., Arnold, J.R., Brekke, L.D., 2016. Characterizing Uncertainty of the Hydrologic Impacts of Climate Change. Curr. Clim. Chang. Reports. https://doi.org/10.1007/s40641-016-0034-x

Croke, B.F.W., Jakeman, A.J., 2004. A catchment moisture deficit module for the IHACRES rainfall-runoff model. Environ. Model. Softw. https://doi.org/10.1016/j.envsoft.2003.09.001

Déqué, M., Rowell, D.P., Lüthi, D., Giorgi, F., Christensen, J.H., Rockel, B., Jacob, D., Kjellström, E., De Castro, M., Van Den Hurk, B., 2007. An intercomparison of regional climate simulations for Europe: Assessing uncertainties in model projections. Clim. Change. https://doi.org/10.1007/s10584-006-9228-x

Descroix, L., Mahé, G., Lebel, T., Favreau, G., Galle, S., Gautier, E., Olivry, J.C., Albergel, J., Amogu, O., Cappelaere, B., Dessouassi, R., Diedhiou, A., Le Breton, E., Mamadou, I., Sighomnou, D., 2009. Spatio-temporal variability of hydrological regimes around the boundaries between Sahelian and Sudanian areas of West Africa: A synthesis. J. Hydrol. 375, 90–102. https://doi.org/10.1016/j.jhydrol.2008.12.012

Dezetter, A., Girard, S., Paturel, J.E., Mahé, G., Ardoin-Bardin, S., Servat, E., 2008. Simulation of runoff in West Africa: Is there a single data-model combination that produces the best simulation results? J. Hydrol. https://doi.org/10.1016/j.jhydrol.2008.03.014

Dieppois, B., Diedhiou, A., Durand, A., Fournier, M., Massei, N., Sebag, D., Xue, Y., Fontaine, B., 2013. Quasi-decadal signals of Sahel rainfall and West African monsoon since the mid-twentieth century. J. Geophys. Res. Atmos. 118, 12587–12599. https://doi.org/10.1002/2013JD019681

Dieppois, B., Durand, A., Fournier, M., Diedhiou, A., Fontaine, B., Massei, N., Nouaceur, Z., Sebag, D., 2015. Low-frequency variability and zonal contrast in Sahel rainfall and Atlantic sea surface temperature teleconnections during the last century. Theor. Appl. Climatol. 121, 139–155. https://doi.org/10.1007/s00704-014-1229-5

Dieppois, B., Pohl, B., Cretat, J., Eden, J., Sidibe, M., New, M., Rouault, M., Lawler, D.,2019. Clim. Dyn.https://doi.org/10.1007/s00382-019-04720-5.

Dieulin, C., Mahé, G., Paturel, J. E., Ejjiyar, S., Tramblay, Y., Rouché, N., & EL Mansouri, B. (2019). A New 60-Year 1940/1999 Monthly-Gridded Rainfall Data Set for Africa. *Water*, *11*(2), 387.

Droogers, P., Allen, R.G., 2002. Estimating reference evapotranspiration under inaccurate data conditions. Irrig. Drain. Syst. https://doi.org/10.1023/A:1015508322413

Druyan, L.M., Feng, J., Cook, K.H., Xue, Y., Fulakeza, M., Hagos, S.M., Konaré, A., Moufouma-Okia, W., Rowell, D.P., Vizy, E.K., Ibrah, S.S., 2010. The WAMME regional model intercomparison study. Clim. Dyn. 35, 175–192. https://doi.org/10.1007/s00382-009-0676-7

Eden, J.M., Widmann, M., Grawe, D., Rast, S., 2012. Skill, correction, and downscaling of GCM-simulated precipitation. J. Clim. https://doi.org/10.1175/JCLI-D-11-00254.1

Eyring, V., Cox, P. M., Flato, G. M., Gleckler, P. J., Abramowitz, G., Caldwell, P., ... & Hurtt, G. C. (2019). Taking climate model evaluation to the next level. *Nature Climate Change*, *9*(2), 102-110.

Funk, C., Michaelsen, J., Marshall, M.T., 2012. Mapping recent decadal climate variations in precipitation and temperature across eastern Africa and the sahel, in: Remote Sensing of Drought: Innovative Monitoring Approaches. https://doi.org/10.1201/b11863

Geisser, S., 1975. The predictive sample reuse method with applications. J. Am. Stat. Assoc. https://doi.org/10.1080/01621459.1975.10479865

Giannini, A., Saravanan, R., Chang, P., 2003. Oceanic Forcing of Sahel Rainfall on Interannual to Interdecadal Time Scales. Science (80-.). 302, 1027–1030. https://doi.org/10.1126/science.1089357

Giorgi, F., Jones, C., Asrar, G.R., 2009. Addressing climate information needs at the regional level: The CORDEX framework. World Meteorol. Organ. Bull. https://doi.org/10.1109/ICASSP.2009.4960141

Giuntoli, I., Villarini, G., Prudhomme, C., Hannah, D. M., 2018. Uncertainties in projected runoff over the conterminous United States. *Climatic change*, *150*(3-4), 149-162.

Gudmundsson, L., Bremnes, J.B., Haugen, J.E., Engen-Skaugen, T., 2012. Technical Note: Downscaling RCM precipitation to the station scale using statistical transformations – A comparison of methods. Hydrol. Earth Syst. Sci. https://doi.org/10.5194/hess-16-3383-2012

Hargreaves, G.H., Samani, Z., 1985. Reference crop evapotranspiration from temperature. Appl. Eng. Agric. https://doi.org/10.13031/2013.26773

Harris, I., Jones, P.D., Osborn, T.J., Lister, D.H., 2014. Updated high-resolution grids of monthly climatic observations - the CRU TS3.10 Dataset. Int. J. Climatol. 34, 623–642. https://doi.org/10.1002/joc.3711

Hattermann, F.F., Vetter, T., Breuer, L., Su, B., Daggupati, P., Donnelly, C., Fekete, B., Florke, F., Gosling, S.N., Hoffmann, P., Liersch, S., Masaki, Y., Motovilov, Y., Muller, C., Samaniego, L., Stacke, T., Wada, Y., Yang, T., Krysnaova, V., 2018. Sources of uncertainty in hydrological climate impact assessment: A cross-scale study. Environ. Res. Lett. https://doi.org/10.1088/1748-9326/aa9938

Hawkins, E., Sutton, R., 2009. The potential to narrow uncertainty in regional climate predictions. *Bulletin of the American Meteorological Society*, *90*(8), 1095-1108.

Hempel, S., Frieler, K., Warszawski, L., Schewe, J., Piontek, F., 2013. A trend-preserving bias correction – the ISI-MIP approach. Earth Syst. Dyn. 4, 219–236. https://doi.org/10.5194/esd-4-219-2013

Hingray, B., Saïd, M., 2014. Partitioning internal variability and model uncertainty components in a multimember multi-model ensemble of climate projections. *Journal of Climate*, *27*(17), 6779-6798.

Huang, B., Thorne, P.W., Banzon, V.F., Boyer, T., Chepurin, G., Lawrimore, J.H., Menne, M.J., Smith, T.M., Vose, R.S., Zhang, H.M., 2017. Extended reconstructed Sea surface temperature, Version 5 (ERSSTv5): Upgrades, validations, and intercomparisons. J. Clim. 30, 8179–8205. https://doi.org/10.1175/JCLI-D-16-0836.1

Ibrahim, B., Karambiri, H., Polcher, J., 2015. Hydrological Impacts of the Changes in Simulated Rainfall Fields on Nakanbe Basin in Burkina Faso. Climate 3, 442–458. https://doi.org/10.3390/cli3030442

IPCC, 2013. Climate Change 2013: The Physical Science Basis. Contribution of Working Group I to the Fifth Assessment Report of the Intergovernmental Panel on Climate Change [Stocker, T.F., D. Qin, G.-K. Plattner, M. Tignor, S.K. Allen, J. Boschung, A. Nauels, Y. Xia, V. Bex and P.M. Midgley (eds.)]. Cambridge University Press, Cambridge, United Kingdom and New York, NY, USA.

IPCC, 2014. Climate Change 2014: Synthesis Report. Contribution of Working Groups I, II and III to the Fifth Assessment Report of the Intergovernmental Panel on Climate Change, Core Writing Team, R.K. Pachauri and L.A. Meyer. https://doi.org/10.1017/CBO9781107415324.004

Jakeman, A.J., Hornberger, G.M., 1993. How much complexity is warranted in a rainfall-runoff model? Water Resour. Res. https://doi.org/10.1029/93WR00877

Jakeman, A.J., Littlewood, I.G., Whitehead, P.G., 1990. Computation of the instantaneous unit hydrograph and identifiable component flows with application to two small upland catchments. J. Hydrol. https://doi.org/10.1016/0022-1694(90)90097-H

Kauffeldt, A., Wetterhall, F., Pappenberger, F., Salamon, P., Thielen, J., 2016. Technical review of large-scale hydrological models for implementation in operational flood forecasting schemes on continental level. Environ. Model. Softw. https://doi.org/10.1016/j.envsoft.2015.09.009

Kebe, I., Sylla, M. B., Omotosho, J. A., Nikiema, P. M., Gibba, P., Giorgi, F., 2017. Impact of GCM boundary forcing on regional climate modeling of West African summer monsoon precipitation and circulation features. *Climate Dynamics*, *48*(5-6), 1503-1516.

Kingston, D.G., Fleig, A.K., Tallaksen, L.M., Hannah, D.M., 2013. Ocean–Atmosphere Forcing of Summer Streamflow Drought in Great Britain. J. Hydrometeorol. 14, 331–344. https://doi.org/10.1175/JHM-D-11-0100.1

Kling, H., Fuchs, M., Paulin, M., 2012. Runoff conditions in the upper Danube basin under an ensemble of climate change scenarios. J. Hydrol. 424–425, 264–277. https://doi.org/10.1016/j.jhydrol.2012.01.011

Lin, J.L., 2007. The double-ITCZ problem in IPCC AR4 coupled GCMs: Ocean-atmosphere feedback analysis. J. Clim. https://doi.org/10.1175/JCLI4272.1

Mahé, G., Bamba, F., Soumaguel, A., Orange, D., Olivry, J.C., 2009. Water losses in the inner delta of the River Niger: Water balance and flooded area. Hydrol. Process. https://doi.org/10.1002/hyp.7389

Mahé, G., L'Hote, Y., Olivry, J.C., Wotling, G., 2001. Trends and discontinuities in regional rainfall of West and Central Africa: 1951–1989. Hydrol. Sci. J. 46, 211–226. https://doi.org/10.1080/02626660109492817

Mahe, G., Paturel, J.E., Servat, E., Conway, D., Dezetter, A., 2005. The impact of land use change on soil water holding capacity and river flow modelling in the Nakambe River, Burkina-Faso. J. Hydrol. https://doi.org/10.1016/j.jhydrol.2004.04.028

Maraun, D., 2012. Nonstationarities of regional climate model biases in European seasonal mean temperature and precipitation sums. Geophys. Res. Lett. https://doi.org/10.1029/2012GL051210

Mascaro, G., White, D.D., Westerhoff, P., Bliss, N., 2015. Performance of the CORDEX-Africa regional climate simulations in representing the hydrological cycle of the Niger river basin. J. Geophys. Res. https://doi.org/10.1002/2015JD023905

Massei, N., Dieppois, B., Hannah, D.M., Lavers, D.A., Fossa, M., Laignel, B., Debret, M., 2017. Multi-time-scale hydroclimate dynamics of a regional watershed and links to large-scale atmospheric circulation: Application to the Seine river catchment, France. J. Hydrol. https://doi.org/10.1016/j.jhydrol.2017.01.008

Mba, W.P., Longandjo, G.N.T., Moufouma-Okia, W., Bell, J.P., James, R., Vondou, D.A., Haensler, A., Fotso-Nguemo, T.C., Guenang, G.M., Tchotchou, A.L.D., Kamsu-Tamo, P.H., Takong, R.R., Nikulin, G., Lennard, C.J., Dosio, A., 2018. Consequences of 1.5 °c and 2 °c global warming levels for temperature and precipitation changes over Central Africa. Environ. Res. Lett. https://doi.org/10.1088/1748-9326/aab048

Mbaye, M.L., Hagemann, S., Haensler, A., Stacke, T., Gaye, A.T., Afouda, A., 2015. Assessment of Climate Change Impact on Water Resources in the Upper Senegal Basin (West Africa). Am. J. Clim. Chang. https://doi.org/10.4236/ajcc.2015.41008

Michel, C., 1989. Hydrologie appliquée aux petits bassins versants ruraux [WWW Document]. Cemagref, Antony.

Mohino, E., Janicot, S., Bader, J., 2011. Sahel rainfall and decadal to multi-decadal sea surface temperature variability. Clim. Dyn. https://doi.org/10.1007/s00382-010-0867-2

Monerie, P.A., Fontaine, B., Roucou, P., 2012. Expected future changes in the African monsoon between 2030 and 2070 using some CMIP3 and CMIP5 models under a medium-low RCP scenario. J. Geophys. Res. Atmos. https://doi.org/10.1029/2012JD017510

Moss, R.H., Edmonds, J.A., Hibbard, K.A., Manning, M.R., Rose, S.K., Van Vuuren, D.P., Carter, T.R., Emori, S., Kainuma, M., Kram, T., Meehl, G.A., Mitchell, J.F.B., Nakicenovic, N., Riahi, K., Smith, S.J., Stouffer, R.J., Thomson, A.M., Weyant, J.P., Wilbanks, T.J., 2010. The next generation of scenarios for climate change research and assessment. Nature. https://doi.org/10.1038/nature08823

Mouelhi, S., Michel, C., Perrin, C., Andréassian, V., 2006. Stepwise development of a two-parameter monthly water balance model. J. Hydrol. https://doi.org/10.1016/j.jhydrol.2005.06.014

Mtongori, H.I., Stordal, F., Benestad, R.E., 2016. Evaluation of empirical statistical downscaling models' skill in predicting Tanzanian rainfall and their application in providing future downscaled scenarios. J. Clim. https://doi.org/10.1175/JCLI-D-15-0061.1

Nash, J.E., Sutcliffe, J. V, 1970. River Flow Forecasting Through Conceptual Models Part I-a Discussion of Principles*. J. Hydrol. 10, 282–290. https://doi.org/10.1016/0022-1694(70)90255-6

New, M., Hulme, M., Jones, P., 2000. Representing twentieth-century space-time climate variability. Part II: Development of 1901-96 monthly grids of terrestrial surface climate. J. Clim. https://doi.org/10.1175/1520-0442(2000)013<2217:RTCSTC>2.0.CO;2

Nicholson, S.E., 2013. The West African Sahel: A Review of Recent Studies on the Rainfall Regime and Its Interannual Variability. ISRN Meteorol. 2013, 1–32. https://doi.org/10.1155/2013/453521

Nicholson, S.E., 2008. The intensity, location and structure of the tropical rainbelt over west Africa as factors in interannual variability. Int. J. Climatol. https://doi.org/10.1002/joc.1507

Niel, H., Paturel, J.E., Servat, E., 2003. Study of parameter stability of a lumped hydrologic model in a context of climatic variability. J. Hydrol. https://doi.org/10.1016/S0022-1694(03)00158-6

Nikulin, G., Jones, C., Giorgi, F., Asrar, G., Büchner, M., Cerezo-Mota, R., Christensen, O.B., Déqué, M., Fernandez, J., Hänsler, A., van Meijgaard, E., Samuelsson, P., Sylla, M.B., Sushama, L., 2012. Precipitation climatology in an ensemble of CORDEX-Africa regional climate simulations. J. Clim. https://doi.org/10.1175/JCLI-D-11-00375.1

Oyerinde, G., Wisser, D., Hountondji, F., Odofin, A., Lawin, A., Afouda, A., Diekkrüger, B., 2016. Quantifying Uncertainties in Modeling Climate Change Impacts on Hydropower Production. Climate. https://doi.org/10.3390/cli4030034

Paturel, J. E., Ouedraogo, M., Mahé, G., Servat, E., Dezetter, A., Ardoin, S., 2003. The influence of distributed input data on the hydrological modelling of monthly river flow regimes in West Africa. *Hydrological sciences journal*, *48*(6), 881-890.

Paturel, J.E., Servat, E., Vassiliadis, A., 1995. Sensitivity of conceptual rainfall-runoff algorithms to errors in input data - case of the GR2M model. J. Hydrol. https://doi.org/10.1016/0022-1694(94)02654-T

Percival, D.B., Walden, A.T., 2000. Wavelet Methods for Time Series Analysis, Cambridge University Press. https://doi.org/10.1198/tech.2001.s49

Ringard, J., Dieppois, B., Rome, S., Diedhiou, A., Pellarin, T., Konaré, A., Diawara, A., Konaté, D., Dje, B.K., Katiellou, G.L., Seidou Sanda, I., Hassane, B., Vischel, T., Garuma, G.F., Mengistu, G., Camara, M., Diongue, A., Gaye, A.T., Descroix, L., 2016. The intensification of thermal extremes in west Africa. Glob. Planet. Change 139, 66–77. https://doi.org/10.1016/j.gloplacha.2015.12.009

Robin, Y., Vrac, M., Naveau, P., Yiou, P., 2019. Multivariate stochastic bias corrections with optimal transport. *Hydrology and Earth System Sciences*, *23*(2), 773-786.

Rodríguez-Fonseca, B., Mohino, E., Mechoso, C.R., Caminade, C., Biasutti, M., Gaetani, M., Garcia-Serrano, J., Vizy, E.K., Cook, K., Xue, Y., Polo, I., Losada, T., Druyan, L., Fontaine, B., Bader, J., Doblas-Reyes, F.J., Goddard, L., Janicot, S., Arribas, A., Lau, W., Colman, A., Vellinga, M., Rowell, D.P., Kucharski, F., Voldoire, A., 2015. Variability and predictability of west African droughts: A review on the role of sea surface temperature anomalies. J. Clim. 28, 4034–4060. https://doi.org/10.1175/JCLI-D-14-00130.1

Roudier, P., Ducharne, A., Feyen, L., 2014. Climate change impacts on runoff in West Africa: A review. Hydrol. Earth Syst. Sci. https://doi.org/10.5194/hess-18-2789-2014

Salack, S., Sarr, B., Sangare, S.K., Ly, M., Sanda, I.S., Kunstmann, H., 2015. Crop-climate ensemble scenarios to improve risk assessment and resilience in the semi-arid regions of West Africa. Clim. Res. https://doi.org/10.3354/cr01282

Sarr, A., 2017. Multi-Scale Characteristics of Precipitation and Temperature over West Africa Using SMHI-RCA Driven by GCMs under RCP8.5. Am. J. Clim. Chang. https://doi.org/10.4236/ajcc.2017.63024

Serdeczny, O., Adams, S., Baarsch, F., Coumou, D., Robinson, A., Hare, W., Schaeffer, M., Perrette, M., Reinhardt, J., 2017. Climate change impacts in Sub-Saharan Africa: from physical changes to their social repercussions. Reg. Environ. Chang. https://doi.org/10.1007/s10113-015-0910-2

Sidibe, M., Dieppois, B., Mahé, G., Paturel, J.E., Amoussou, E., Anifowose, B., Lawler, D., 2018. Trend and variability in a new, reconstructed streamflow dataset for West and Central Africa, and climatic interactions, 1950–2005. J. Hydrol. https://doi.org/10.1016/j.jhydrol.2018.04.024

Sidibe, M., Dieppois, B., Eden, J., Mahé, G., Paturel, J. E., Amoussou, E., Anifowose, B., Lawler, D., 2019. Interannual to Multi-decadal streamflow variability in West and Central Africa: Interactions with catchment properties and large-scale climate variability. *Global and Planetary Change*. https://doi.org/10.1016/j.gloplacha.2019.04.003

Stanzel, P., Kling, H., Bauer, H., 2018. Climate change impact on West African rivers under an ensemble of CORDEX climate projections. Clim. Serv. https://doi.org/10.1016/j.cliser.2018.05.003

Steinschneider, S., Wi, S., Brown, C., 2015. The integrated effects of climate and hydrologic uncertainty on future flood risk assessments. Hydrol. Process. 29, 2823–2839. https://doi.org/10.1002/hyp.10409

Sterling, S.M., Ducharne, A., Polcher, J., 2013. The impact of global land-cover change on the terrestrial water cycle. Nat. Clim. Chang. https://doi.org/10.1038/nclimate1690

Stone, M., 1974. Cross-validation and multinomial prediction. Biometrika.

https://doi.org/10.1093/biomet/61.3.509

Sultan, B., Janicot, S., 2000. Abrupt shift of the ITCZ over West Africa and intra-seasonal variability. Geophys. Res. Lett. https://doi.org/10.1029/1999GL011285

Sylla, M.B., Nikiema, P.M., Gibba, P., Kebe, I., Klutse, N.A.B., 2016. Climate change over West Africa: Recent trends and future projections, in: Adaptation to Climate Change and Variability in Rural West Africa. https://doi.org/10.1007/978-3-319-31499-0_3

Sylla, M.B., Pal, J.S., Faye, A., Dimobe, K., Kunstmann, H., 2018. Climate change to severely impact West African basin scale irrigation in 2 °C and 1.5 °C global warming scenarios. Sci. Rep. https://doi.org/10.1038/s41598-018-32736-0

Taylor, K.E., Stouffer, R.J., Meehl, G.A., 2012. An overview of CMIP5 and the experiment design. Bull. Am. Meteorol. Soc. https://doi.org/10.1175/BAMS-D-11-00094.1

Teutschbein, C., Seibert, J., 2012. Bias correction of regional climate model simulations for hydrological climate-change impact studies: Review and evaluation of different methods. J. Hydrol. https://doi.org/10.1016/j.jhydrol.2012.05.052

Wang, C., Zhang, L., Lee, S.K., Wu, L., Mechoso, C.R., 2014. A global perspective on CMIP5 climate model biases. Nat. Clim. Chang. https://doi.org/10.1038/nclimate2118

Washington, R., James, R., Pearce, H., Pokam, W.M., Moufouma-Okia, W., 2013. Congo basin rainfall climatology: Can we believe the climate models? Philos. Trans. R. Soc. B Biol. Sci. https://doi.org/10.1098/rstb.2012.0296

Wilcke, R. A. I., T. Mendlik, and A. Gobiet, 2013: Multi-variable error correction of regional climate models.Climatic Change,120, 871–887. https://doi.org/10.1007/s10584-013-0845-x

Yira, Y., Diekkrüger, B., Steup, G., Yaovi Bossa, A., 2017. Impact of climate change on hydrological conditions in a tropical West African catchment using an ensemble of climate simulations. Hydrol. Earth Syst. Sci. https://doi.org/10.5194/hess-21-2143-2017

Zaré, A., Mahé, G., Paturel, J.E., Barbier, B., 2017. Influence du Bani sur la variabilité saisonnière et interannuelle de la crue du fleuve Niger dans le delta intérieur au Mali. Hydrol. Sci. J. https://doi.org/10.1080/02626667.2016.1148816

Appendix A: List of selected stations with model performances and multi-model ensemble relative change in streamflow under RCP4.5 emission scenario

Station Metadata						Model calibration (KGE)			Relative Change (MME)		
ID	**Basin**	**Station**	**Area(km2)**	**LAT**	**LON**	**GR2M**	**IHACRES**	**SST-Q**	**GR2M**	**IHACRES**	**SST-Q**
BFQ0010	LERABA	YENDERE au pont	6288	10.167	-5.068	0.85	0.7	0.46	0.157	0.107	-0.02
BFQ0060	VOLTA	WAYEN	20241	12.379	-1.08	0.83	0.7	0.26	0.287	0.233	0.295
BFQ0064	VOLTA	BOROMO	54499	11.783	-2.917	0.74	0.72	0.47	0.202	0.1	0.126
BFQ0065	VOLTA	DAPOLA	86566	10.567	-2.917	0.91	0.91	0.39	0.212	0.132	-0.07
BFQ0072	VOLTA	NWOKUY	15463.75	12.528	-3.55	0.75	0.81	0.64	0.144	0.123	0.174
BFQ0074	VOLTA	SAMANDENI	4454	11.467	-4.467	0.91	0.87	0.43	0.157	0.094	0.142
BJQ0009	SOTA	COUBERI	25974	11.74	3.333	0.89	0.77	0.54	0.115	0.063	0.127
BJQ0022	COUFFO	LANHOUNTA - LANTA	1701.517	7.1	1.883	0.8	0.7	0.4	0.08	0.003	0.315
BJQ0033	OUEME	BONOU	48816	6.9	2.45	0.9	0.66	0.61	0.097	0.023	0.419
BJQ0036	OUEME	HETIN SOTA	49907.33	6.6	2.5	0.7	0.61	0.61	0.042	0.09	0.09
BJQ0047	OKPARA	KABOUA	10430	8.25	2.717	0.79	0.44	0.55	0.08	0.005	0.338
BJQ0050	SOTA	RTE KANDI-SEGBANA AMONT	8426	10.983	3.25	0.86	0.69	0.49	0.101	0.015	0.146
BJQ1000	PENDJARI	PORGA	22920	10.994	0.977	0.84	0.8	0.42	0.163	0.063	0.077
BJQ2000	NIGER	MALANVILLE	719331	11.888	3.383	0.53	0.82	0.5	0.15	0.059	-0.07
BJQ2004	OUEME	PONT DE BETEROU	10491	9.199	2.268	0.84	0.83	0.49	0.087	0.044	0.314
BJQ2005	OUEME	PONT DE SAVE	23476	8	2.417	0.82	0.86	0.55	0.1	0.139	0.442
CFQ0025	OUBANGUI	ZINGA TRANSIT	526113	3.714	18.587	0.85	0.93	0.49	-0.03	0.001	0.069
CFQ0027	MBOMOU	ZEMIO	27952	5.029	25.147	0.76	0.81	0.47	-0.07	-0.068	0.091
CFQ0028	BANGUI-KETTE	ALINDAO	4551	5.045	21.202	0.58	0.85	0.45	-0	-0.04	0.155
CFQ0034	LOBAYE	M'BATA	31346	3.666	21.981	-0.21	0.88	0.52	0.006	-0.03	-0.02
CFQ0040	M'POKO	BOSSELE-BALI	10573.43	4.531	18.469	0.84	0.83	0.47	0.014	-0.056	0.148
CFQ0057	SANGHA	SALO	72416	3.182	16.114	0.44	0.89	0.44	0.002	-0.047	-0.01

CFQ2000	OUBANGUI	BANGUI	499000	4.364	18.595	0.85	0.92	0.46	-0.03	-0.017	0.068
CGQ0003	ALIMA	TCHIKAPIKA	20067	-1.264	16.169	0.66	0.04	0.73	0.005	0.023	0.004
CGQ0013	LEFINI	BWEMBE	13589	-2.917	15.631	0.1	0.18	0.57	0.005	0.016	0.008
CGQ0014	LIKOUALA	ETOUMBI	4647.94	0.017	14.95	0.71	0.58	0.59	-0.01	-0.035	0.043
CGQ0015	LIKOUALA	MAKOUA	15037.86	0.002	15.633	0.73	0.75	0.62	-0.02	-0.061	-0.13
CGQ0017	N'KENI	GAMBOMA	6202	-1.9	15.85	-0.57	0.14	0.84	0.018	-0.035	0.013
CGQ0020	KOUYOU	LINNEGUE	6890.2	-0.5	15.933	0.49	0.49	0.55	0.002	0.016	0.021
CGQ0026	LIKOUALA	BOTOUALI	19223	-0.55	17.45	0.47	0.87	0.66	0.046	-0.003	0.113
CGQ2000	CONGO	BEACH - V.N. Brazzaville	3700000	-4.273	15.294	0.65	0.85	0.62	-0.03	-0.057	0.05
CGQ2001	SANGHA	OUESSO	159016	1.617	16.05	0.44	0.95	0.45	-0	-0.034	-0.02
CIQ0013	BANDAMA	KIMOUKRO BALISE 10201	56364.5	6.506	-5.305	0.72	0.6	0.41	0.114	0.004	-0.09
CIQ0032	MARAOUE	RTE BEOUMI-SEGUELA - KONGASSO 10145	12905	7.832	-6.254	0.85	0.85	0.52	0.125	0.022	-0.15
CIQ0033	MARAOUE	BOUAFLE 10147	21267	6.98	-5.754	0.84	0.53	0.53	0.124	0.104	-0.1
CIQ0058	NZI	BOCANDA	20880	7.044	-4.52	0.83	0.83	0.5	0.134	-0.006	-0.35
CIQ0061	NZI	DIMBOKRO 10141	24100	6.636	-4.71	0.76	0.72	0.46	0.141	-0.015	-0.29
CIQ0154	KOUROUKELE	IRADOUGOU	1820	9.707	-7.803	0.91	0.74	0.45	0.124	0.177	-0.15
CIQ0292	KAVI	MBESSE	975	5.839	-4.296	0.65	0.4	0.39	0.095	0.06	0.675
CIQ0312	CAVALLY	FLAMPLEU	2508	7.283	-8.058	0.81	0.89	0.52	0.057	-0.012	-0
CIQ0314	CAVALLY	TAI	12719	5.86	-7.45	0.89	0.84	0.56	0.149	0.136	-0.05
CIQ0319	NSE	TAI 1 (TAI PONT)	1424.36	5.875	-7.458	0.75	0.81	0.44	0.16	0.117	-0.07
CIQ4020	BANDAMA	BADA	23809	8.107	-5.497	0.79	0.71	0.46	0.103	-0.015	-0.23
CIQ4022	BANDAMA	TIASSALE 10144	61850	5.895	-4.818	0.78	0.53	0.45	0.113	0.023	-0.33
CIQ4025	NZI	FETEKRO	10175	7.811	-4.688	0.88	0.82	0.49	0.122	-0.031	-0.35
CIQ4026	NZI	MBAHIAKRO 10133	15368	7.446	-4.356	0.84	0.8	0.49	0.124	-0.03	-0.38
CIQ4027	NZI	NZIENOA 10136	35340	5.996	-4.813	0.77	0.74	0.47	0.154	-0.045	-0.44

CIQ4028	COMOE	ANIASSUE PONT 10138	70636	6.638	-3.713	0.81	0.56	0.46	0.155	0.212	-0.34
CIQ4029	COMOE	MBASSO	70500	6.125	-3.48	0.79	0.54	0.49	0.152	0.09	-0.38
CIQ4030	COMOE	SEREBOU	50587	7.938	-3.942	0.84	0.7	0.51	0.162	0.253	-0.27
CIQ4031	SASSANDRA	SEMIEN 10130	29900	7.708	-7.067	0.96	0.87	0.57	0.105	0.053	-0.11
CIQ4032	SASSANDRA	SOUBRE	62173	5.783	-6.613	0.61	0.26	0.41	0.115	0.06	-0.07
CIQ4033	BAFING	BAFINGDALA BIANKOUMA 10162	6049	7.842	-7.667	0.94	0.9	0.79	0.064	-0.007	0.099
CIQ4034	LOBO	NIBEHIBE	6233.53	6.8	-6.7	0.77	0.79	0.37	0.147	0.005	-0.1
CIQ4035	COMOE	AKAKOMOEKRO 10149	57803	7.447	-3.509	0.78	0.6	0.51	0.158	0.151	-0.37
CMQ0029	SANAGA	NACHTIGAL	78625.04	4.35	11.633	0.62	0.86	0.43	0.027	0.009	0.072
CMQ0030	SANAGA	NANGA EBOKO	67600.32	4.7	12.383	0.64	0.88	0.41	0.029	0.017	0.021
CMQ0038	MBAM	BAC DE GOURA	42240.11	4.567	11.367	0.94	0.93	0.53	0.001	-0.015	0.069
CMQ0071	NYONG	DEHANE	26398.84	3.567	10.117	0.55	0.9	0.51	0.001	-0.039	0.061
CMQ5006	BENOUE	BUFFLE NOIR	3309	8.117	13.833	0.91	0.88	0.59	0.096	0.04	0.114
CMQ5007	BENOUE	GAROUA	46940	9.294	13.404	0.89	0.8	0.49	0.061	0.02	0.481
CMQ5015	MAPE	AU PONT DE MAGBA AMONT	4260	5.983	11.267	0.75	0.94	0.42	0.034	-0.011	0.07
CMQ5016	VINA DU SUD	LAHORE	1680	7.25	13.567	0.69	0.92	0.5	0.061	0.125	0.017
CMQ5018	LOBE	BAC KRIBI-CAMPO	3403	2.867	9.883	0.8	0.82	0.35	0.111	0.134	-0.07
CMQ5019	LOKOUNDJE	LOLODORF	1051	3.233	10.733	0.65	0.78	0.54	0.007	-0.032	-0.04
CMQ5038	MUNGO	MUNDAME	2730	4.567	9.533	0.78	0.89	0.63	-0	0.039	0.035
CMQ5040	NTEM	BAC DE NGOAZIK	18100	2.133	11.3	0.83	0.87	0.5	-0.02	-0.008	-0.07
CMQ5044	LOM	BETARE OYA	6931	5.917	14.133	0.7	0.91	0.62	0.027	0.044	0.014
CMQ5047	KIENKE	KRIBI SCIERIE	1533	2.933	9.9	0.73	0.71	0.48	0.145	0.217	-0.17
CMQ5050	KADEI	BATOURI	8974.88	4.417	14.317	0.47	0.87	0.51	-0.01	-0.092	-0.01
GAQ0028	IVINDO	MAKOKOU (LMNG)	35800	0.569	12.861	0.72	0.85	0.56	-0.03	-0.091	-0.02
GAQ0041	NGOUNIE	FOUGAMOU S H O (LMNG)	21620	-1.216	10.591	0.87	0.9	0.32	0.115	0.176	0.088

GAQ0046	NGOUNIE	MOUILA VAL MARIE	14908	-1.887	11.056	0.86	0.85	0.36	0.097	0.144	0.125
GHQ0045	NASIA	NASIA	4968.985	10.15	-0.8	0.84	0.7	0.5	0.125	0.066	-0.27
GNQ0015	NIGER	FARANAH	3171	10.037	-10.749	0.9	0.88	0.45	0.044	0.001	-0.24
GNQ0016	NIGER	KOUROUSSA	17164	10.652	-9.871	0.91	0.89	0.34	0.082	0.124	-0
GNQ0018	NIGER	TIGUIBERY (Siguiri)	6974	11.354	-9.165	0.7	0.93	0.41	0.044	0.115	0.001
GNQ0026	MILO	KANKAN	10047	10.383	-9.3	0.96	0.92	0.25	0.069	0.034	-0.11
GNQ0030	NIANDAN	BARO	1307	10.617	-9.7	0.77	0.95	0.48	0.04	0.029	-0.01
GNQ0034	NIANDAN	KISSIDOUGOU (NIANDAN SCIERIE)	1398	9.25	-10.017	0.76	0.92	0.49	0.045	-0.006	-0.03
GNQ0200	BADI	BAC DE BADI	3095.6	10.283	-13.4	0.86	0.79	0.39	0.014	0.007	-0.05
GNQ0204	KONKOURE	PONT DE LINSAN	1278.69	10.3	-12.417	0.88	0.8	0.35	0.019	0.016	-0.08
MLQ0009	NIGER	DIRE	341047	16.276	-3.395	0.58	0.9	0.52	0.141	0.075	-0.05
MLQ0012	NIGER	KE MACINA	160848	13.958	-5.359	0.93	0.89	0.39	0.108	0.139	0.022
MLQ0019	NIGER	KOULIKORO	120315	12.857	-7.558	0.93	0.92	0.34	0.089	0.072	-0.03
MLQ0022	NIGER	MOPTI	301898	14.496	-4.201	0.85	0.94	0.46	0.142	0.036	-0.06
MLQ0036	NIGER	TOSSAYE	35195	16.933	-0.583	0.27	0.9	0.55	0.076	0.073	0.027
MLQ0091	BANI	SOFARA	130331	14.014	-4.243	0.84	0.93	0.44	0.188	0.135	-0.06
MLQ0123	SENEGAL	GALOUGO	120821	13.833	-11.133	0.92	0.91	0.48	0.142	0.109	0.053
MLQ0130	SENEGAL	BAFING MAKANA	20529	12.55	-10.267	0.84	0.95	0.51	0.057	0.031	0.042
MLQ0131	SENEGAL	SOUKOUTALI	26614	13.2	-10.417	0.96	0.96	0.47	0.078	0.059	0.02
MLQ0134	BAKOYE	OUALIA	78154.91	13.6	-10.383	0.9	0.77	0.38	0.213	0.017	0.171
MLQ0135	BAKOYE	TOUKOTO	16860	13.45	-9.883	0.92	0.75	0.45	0.146	0.075	-0.11
MLQ0137	FALEME	FADOUGOU	8200	12.517	-11.383	0.95	0.92	0.51	0.096	0.074	-0.03
MLQ0145	BAOULE	SIRAMAKANA (Balenda)	51029	13.583	-9.883	0.86	0.76	0.43	0.269	0.018	0.216
MLQ2007	SANKARANI	SELINGUE	6084	11.583	-8.167	0.72	0.72	0.4	0.058	0.004	0.067
MLQ2008	BANI	DOUNA	101225	13.214	-5.903	0.85	0.81	0.42	0.182	0.2	-0.19
MLQ2064	SENEGAL	DAKA SAIDOU	15660	11.95	-10.617	0.97	0.91	0.46	0.061	0.033	-0.03
MLQ2066	SENEGAL	DIBIA	32453	13.233	-10.8	0.9	0.81	0.57	0.083	0.028	0.171

MLQ2069	FALEME	GOURBASSY	16315	13.4	-11.633	0.96	0.73	0.42	0.097	0.052	-0.1
MLQ2070	SENEGAL	KAYES	160835	14.45	-11.45	0.88	0.9	0.5	0.152	0.1	0.07
NEQ2000	NIGER	NIAMEY	631549	13.502	2.105	0.43	0.86	0.54	0.169	0.098	-0.01
NGQ0001	BENUE	MAKURDI	289983	7.75	8.533	0.88	0.92	0.51	0.036	0.036	0.191
NGQ0002	NIGER	ONITSHA	124794	6.167	6.75	0.7	0.91	0.44	0.059	0.047	0.078
NGQ2000	NIGER	LOKOJA	1023616	7.8	6.767	0.91	0.93	0.72	0.117	0.137	0.221
SNQ2039	GAMBIE	KEDOUGOU	8127	12.55	-12.183	0.96	0.95	0.42	0.059	-0.01	0.081
SNQ2045	GAMBIE	MAKO	11007	12.867	-12.35	0.96	0.91	0.46	0.062	0.017	0.121
SNQ2055	GAMBIE	SIMENTI	20936	13.033	-13.3	0.96	0.83	0.51	0.07	0.01	0.118
SNQ2060	GAMBIE	WASSADOU-AMONT	21767	13.35	-13.367	0.95	0.82	0.48	0.069	-0.008	0.1
SNQ2062	GAMBIE	WASSADOU-AVAL	33392	13.35	-13.383	0.93	0.83	0.41	0.085	0.009	0.089
SNQ2063	SENEGAL	BAKEL	220818	14.9	-12.45	0.9	0.91	0.42	0.151	0.026	0.024
SNQ2065	FALEME	KIDIRA UHEA	28703.4	14.455	-12.205	0.96	0.75	0.46	0.112	0.16	-0.01
TDQ0004	CHARI	SARH (EX.FORT-ARCHAMBAULT)	192042.6	9.15	18.417	0.77	0.87	0.4	0.058	0.068	0.084
TDQ0009	CHARI	MAILAO	590607	11.6	15.283	0.76	0.94	0.46	0.066	0.038	0.141
TDQ0013	BAHR-SARA	MANDA	79176.06	9.183	18.2	0.92	0.9	0.44	0.008	-0.011	0.13
TDQ0014	BAHR-SARA	MOISSALA	66467.04	8.333	17.767	0.94	0.89	0.46	0.009	-0.017	0.102
TDQ0036	LIM	OULI BANGALA	4231.94	7.833	15.833	0.9	0.86	0.36	0.128	0.141	-0.04
TDQ0041	PENDE	GORE	11508.84	7.95	16.617	0.86	0.85	0.42	0.053	-0.01	0.244
TDQ0043	TANDJILE	TCHOA	6669.972	9.333	16.083	0.75	0.7	0.39	-0	0.068	0.374
TDQ2011	CHARI	BOUSSO	461854	10.5	16.717	0.84	0.93	0.44	0.07	0.061	0.103
TDQ5004	LOGONE	KATOA	77557	10.833	15.083	0.95	0.96	0.54	0.042	0.034	0.163
TDQ5005	LOGONE	LAI (MISSION)	61010	9.4	16.3	0.95	0.92	0.46	0.053	0.052	0.102
TDQ5006	LOGONE	LOGONE-GANA	3396	11.55	15.15	0.33	0.93	0.53	0.031	0.075	0.159
TOQ0006	KARA	LAMA KARA 1	1502	9.533	1.183	0.88	0.81	0.47	0.062	-0.007	0.132
TOQ0037	SIO	KPEDJI	1824	6.532	1.008	0.85	0.64	0.53	0.002	-0.035	0.075
TOQ0042	MONO	CORREKOPE	9859	7.8	1.3	0.86	0.59	0.59	0.073	0.095	0.143
TOQ0043	MONO	DOTAIKOPE	5797	7.817	1.267	0.85	0.87	0.57	0.068	-0.008	0.123

TOQ0046	MONO	TETETOU	20492	7.017	1.533	0.89	0.72	0.54	0.063	0.071	0.149
TOQ0048	AMOU	AMOU OBLO	197.2919	7.4	0.867	0.8	0.73	0.3	-0	-0.035	0.053
TOQ0053	ANIE	PONT C F T	3688.05	7.733	1.2	0.79	0.72	0.5	0.077	0.019	-0.06
TOQ0059	OGOU	SIRKA	3745	7.917	1.367	0.7	0.7	0.66	0.083	0.124	0.126

List of figures

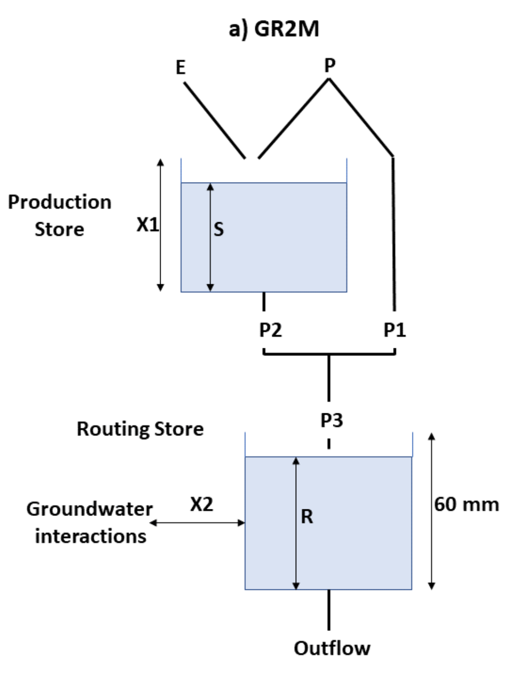

Figure 1:Hydrological model structures a) GR2M hydrological model (adapted from Mouelhi et al. 2006) b) IHACRES-CWI hydrological model (adapted from Jakeman and Hornberger 1993).

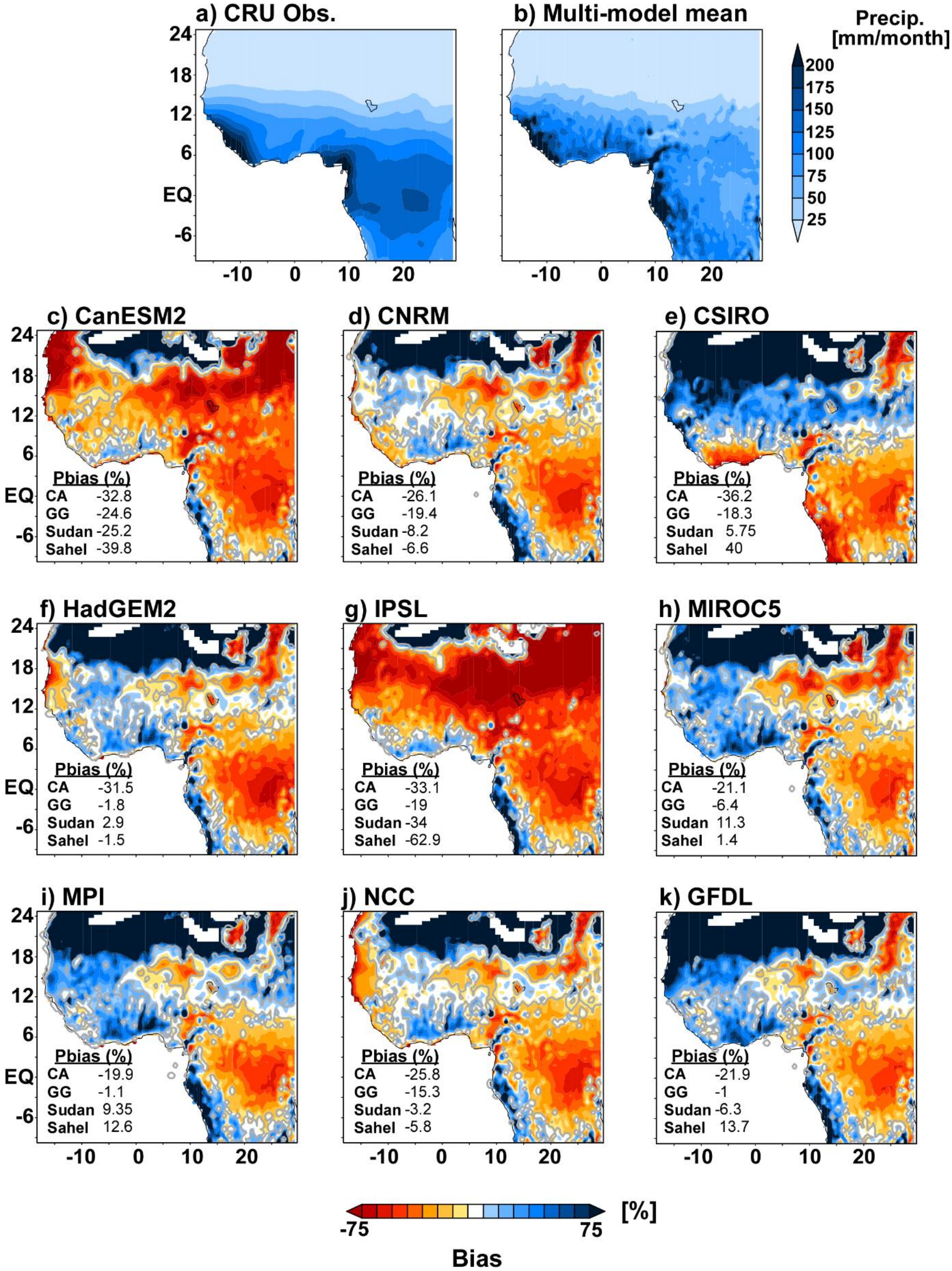

Figure 2: Long-term mean monthly historical precipitation (1951-2005) in (a) CRU observation (b) Multi-model mean. Long-term historical percentage bias between models and CRU precipitation fields (1951-2005) [median pbias is also provided for Central Africa CA, Gulf of Guinea GG, Sudan and Sahel] (c) CanESM2 (d) CNRM (e) CSIRO (f) HadGEM2 (g) IPSL (h) MIROC5 (i) MPI (j) NCC (k) GFDL. Grey contours highlight regions of significant difference between observations and simulations at p≤0.1 based on a t test, applied for each grid-point.

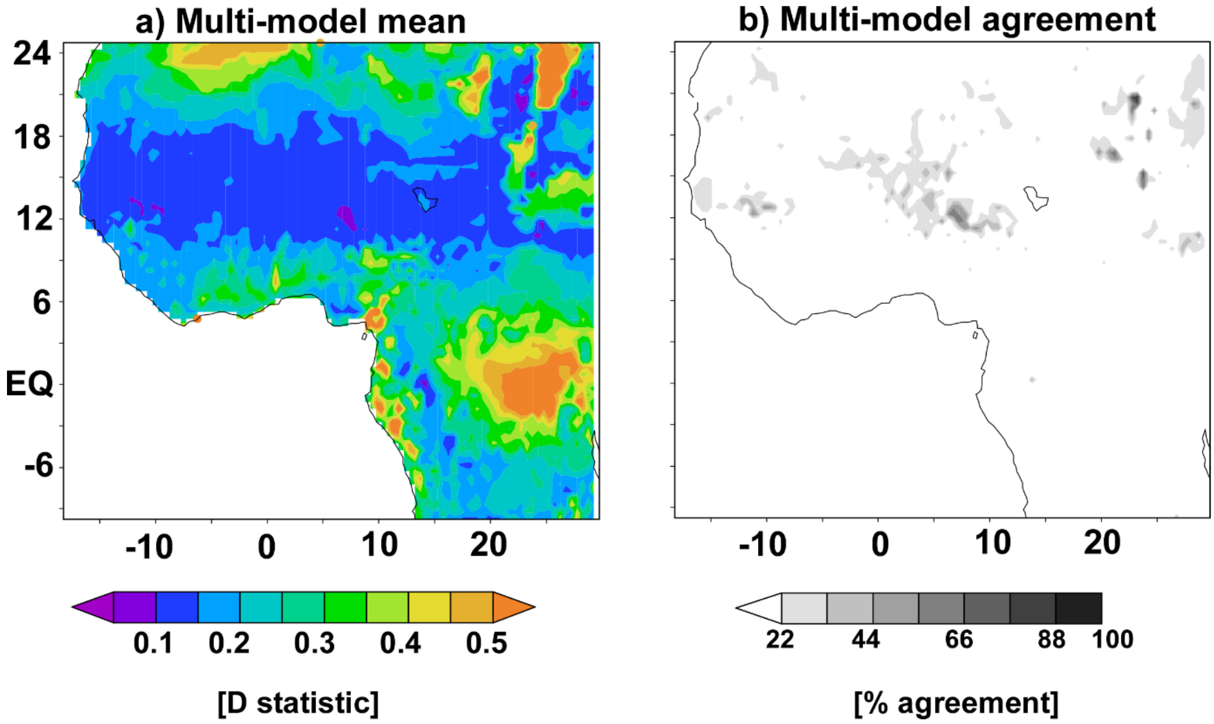

Figure 3: Distributional biases between models and CRU precipitation fields (1951-2005) (a) Multi-model mean K-S test statistic D (b) Models agreement on CDFs similarity at $p \leq 0.1$ significance level based on the KS-test, applied for each grid-point: darker colours correspond to higher model agreement on the similarity in CDFs.

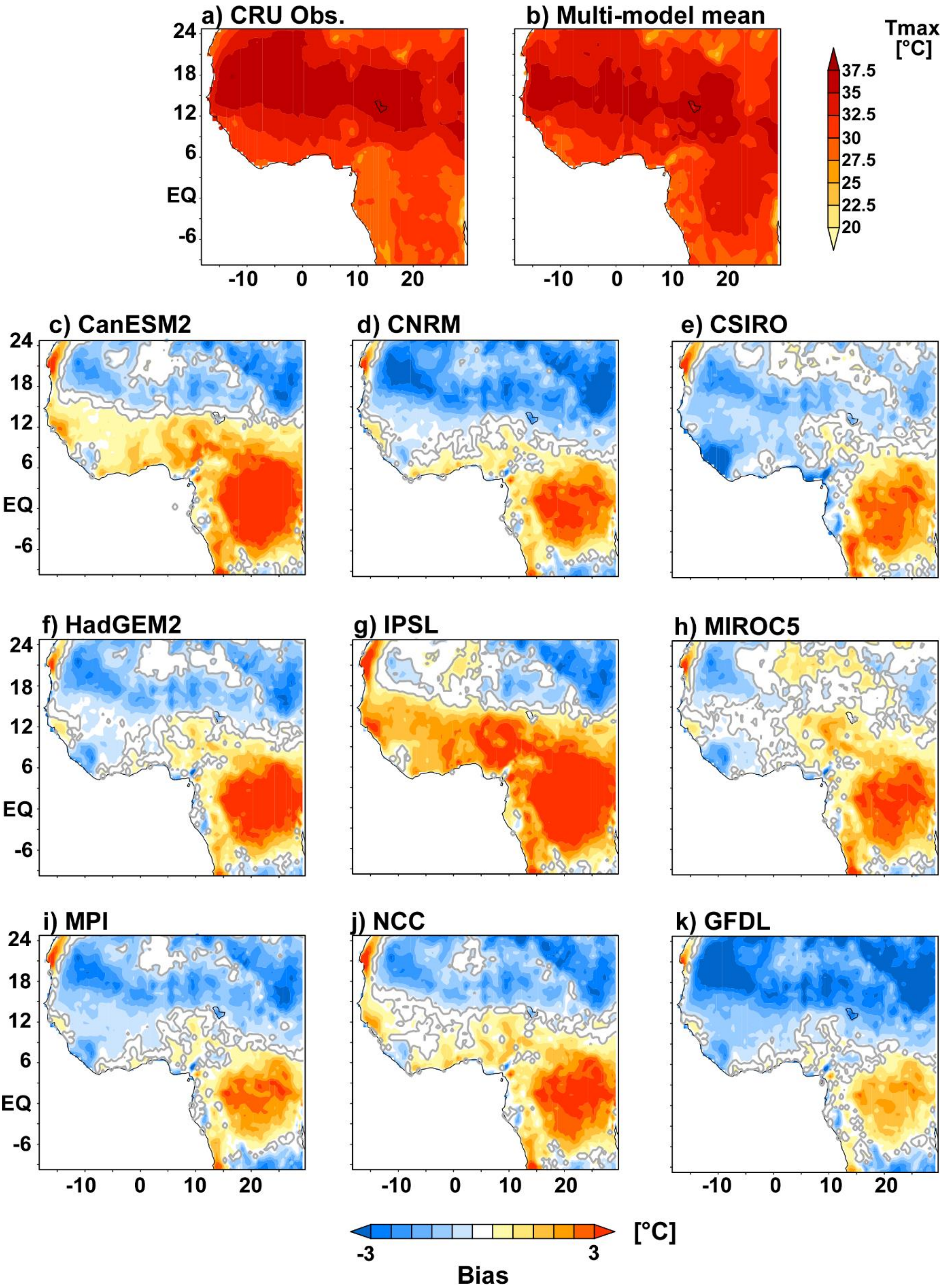

Figure 4: Long-term mean monthly historical maximum temperatures (1951-2005) (a) CRU observation (b) Multi-model mean. Long-term historical absolute bias between models and CRU maximum temperature (c) CanESM2 (d) CNRM (e) CSIRO (f) HadGEM2 (g) IPSL (h) MIROC5 (i) MPI (j) NCC (k) GFDL. Grey contours highlight regions of significant difference between observations and simulations (p≤0.1) based on a t test, applied for each grid-point.

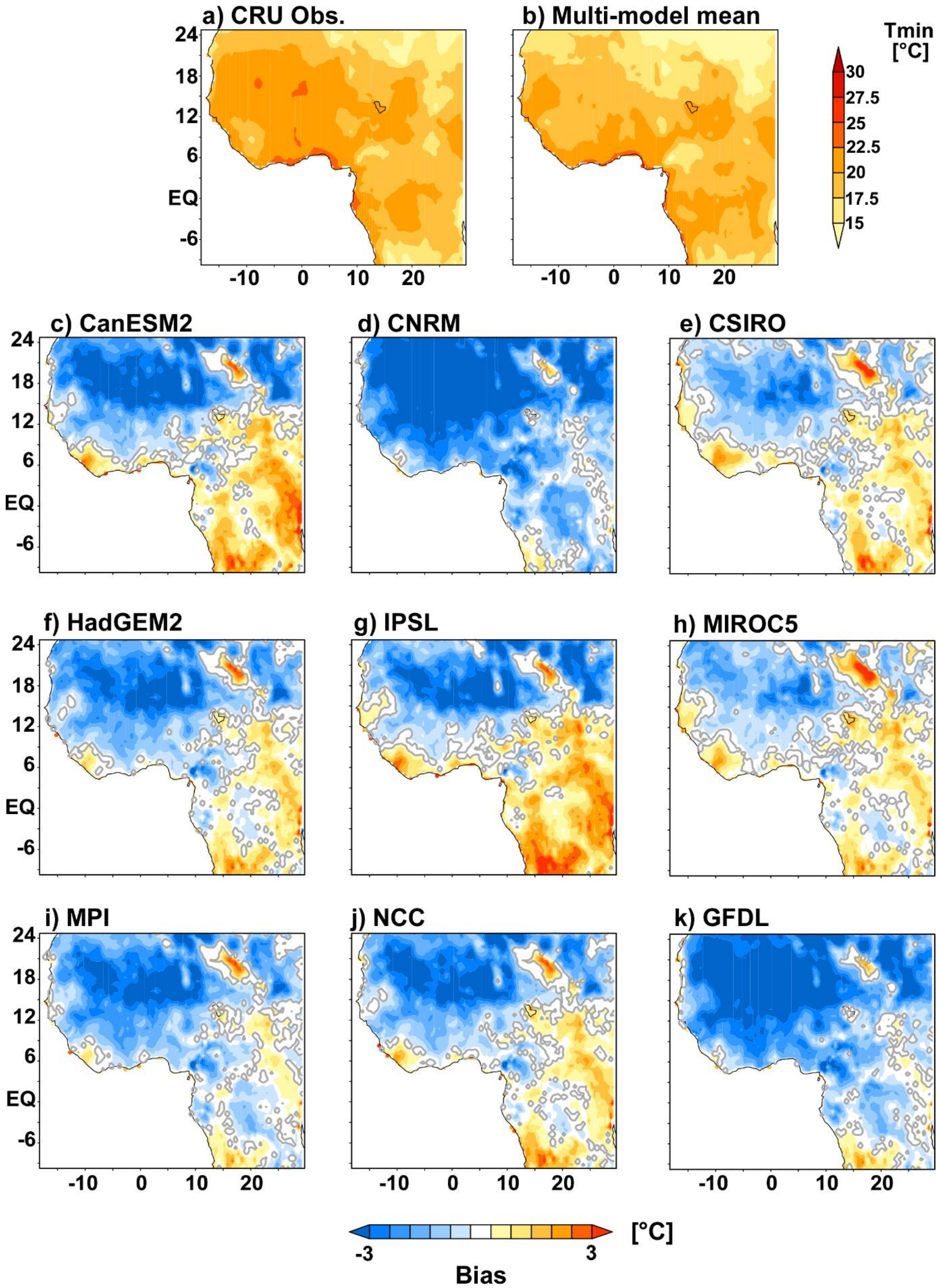

Figure 5: Long-term mean monthly historical minimum temperatures (1951-2005) (a) CRU observation (b) Multi-model mean. Long-term historical absolute bias between models and CRU minimum temperature (c) CanESM2 (d) CNRM (e) CSIRO (f) HadGEM2 (g) IPSL (h) MIROC5 (i) MPI (j) NCC (k) GFDL. Grey contours highlight regions of significant difference between observations and simulations (p≤0.1) based on a t test, applied for each grid-point.

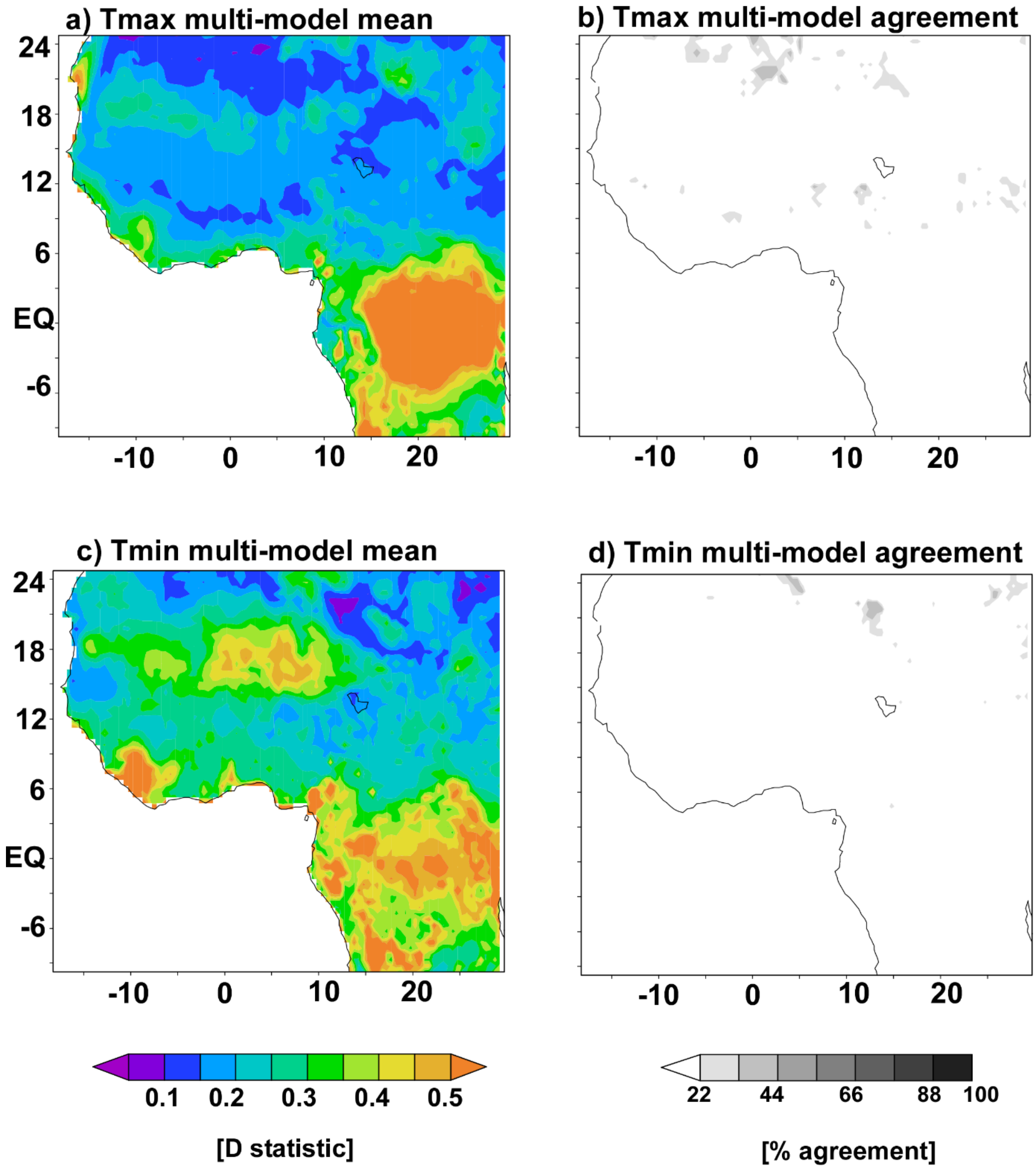

Figure 6: Distributional biases between models and CRU observations (1951-2005) (a-b) Maximum temperatures: (a) Maximum temperature multi-model mean K-S test statistic D (b) Models agreement on CDFs similarity at p ≤ 0.1 significance level based on the KS-test: darker colours correspond to higher model agreement on the similarity in CDFs (c-d) Minimum temperatures: (c) minimum temperature multi-model mean K-S test statistic D (d) Models agreement on CDFs similarity at p ≤ 0.1 significance level based on the KS-test, applied for each grid-point: darker colours correspond to higher model agreement on the similarity in CDFs.

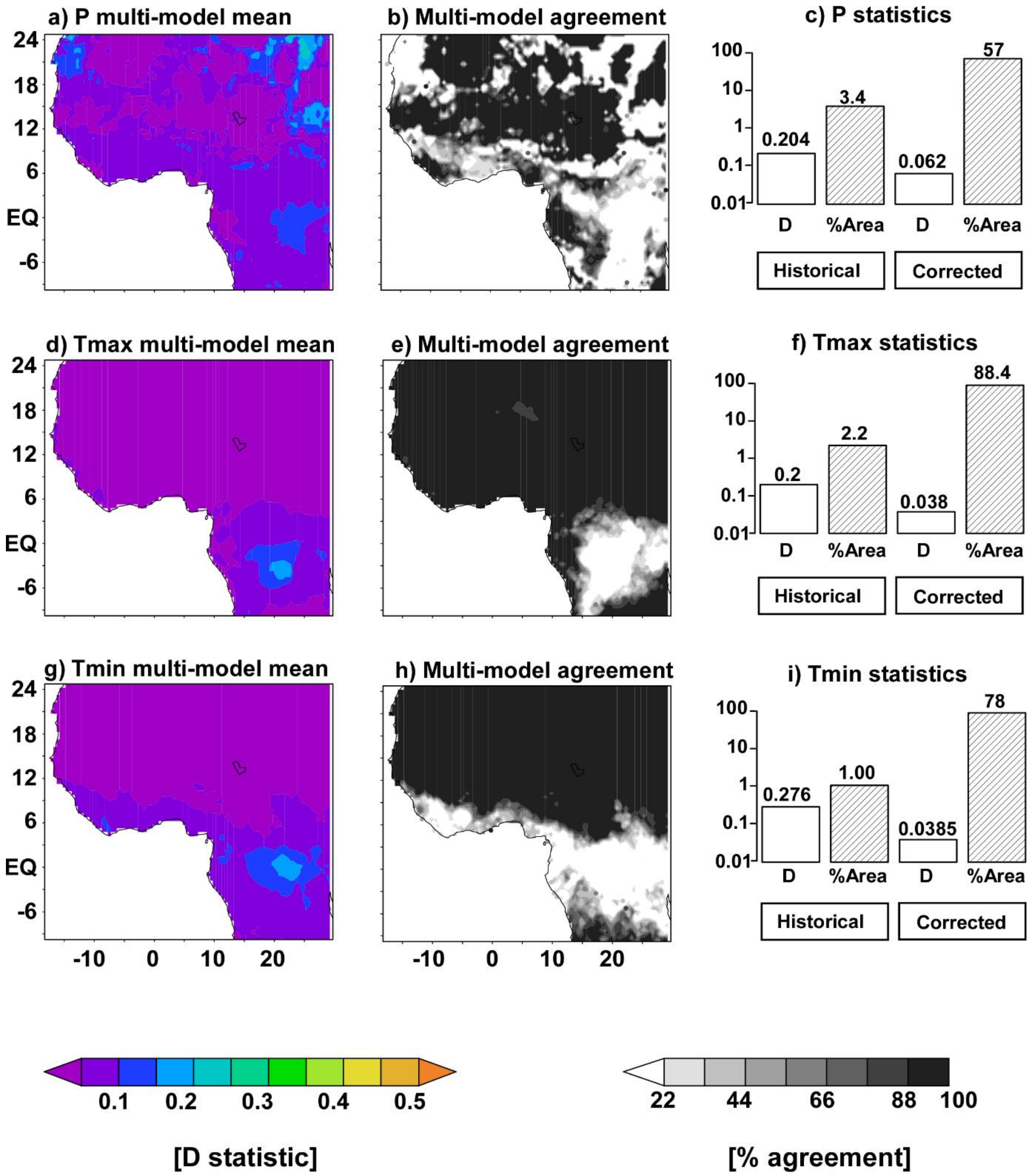

Figure 7: Distributional biases between bias-corrected (cross-validation time series) model simulations and CRU observations (a-c) Precipitation fields: (a) Precipitation multi-model mean K-S test statistic D (b) Models agreement on CDFs similarity at p ≤ 0.1 significance level based on the KS-test, applied for each grid-point (c) Summary of bias correction performances: white histograms refer to the average K-S test statistic D (D); Grey histograms refer to the percentage of area with significantly similar CDFs (%Area) (d-f) Maximum temperature fields (g-i) Minimum temperature fields.

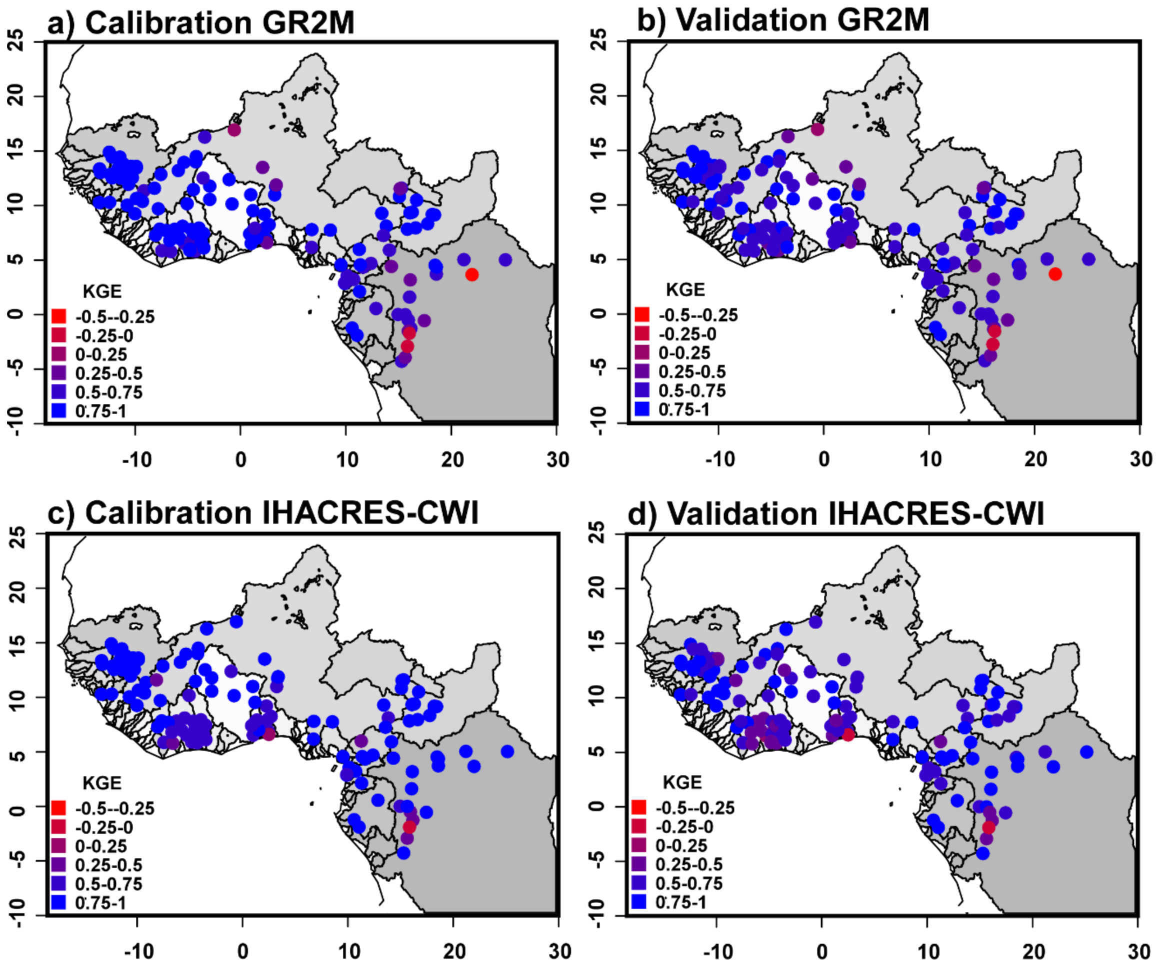

Figure 8: Spatial distribution of hydrological model performances (KGE average for all periods) for calibration and validation periods. Overall average performances for GR2M calibration (a) validation (b). Overall average performances for IHACRES-CWI calibration (c) validation (d). Blue values indicate good performances, while red values indicate poor performances. Grey polygons display the geographic boundaries of the major river basins.

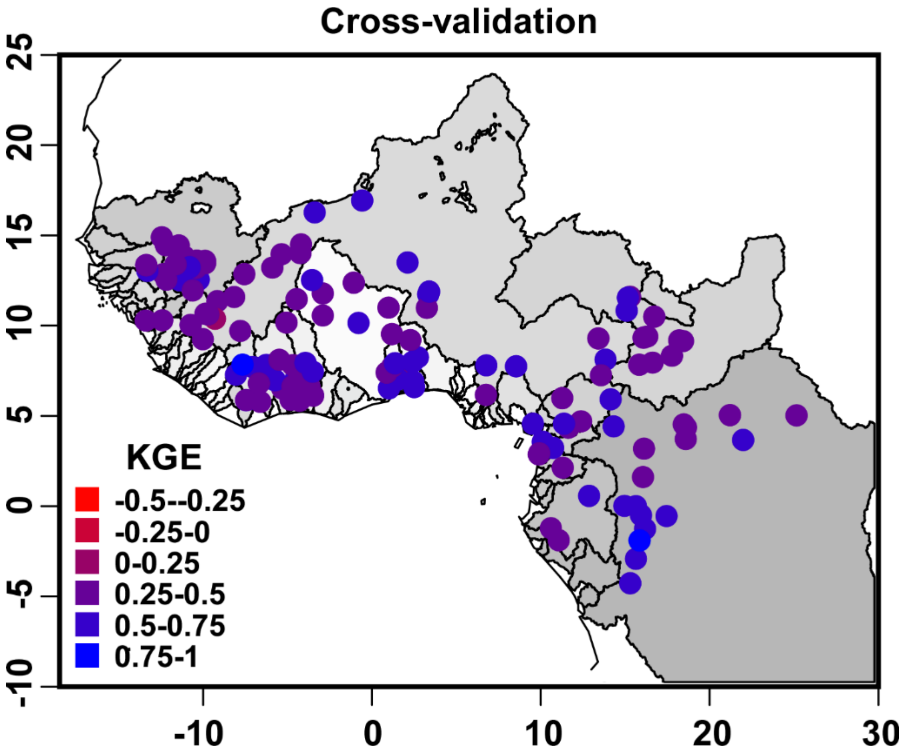

Figure 9: Performance of multi-timescale linear regression models based on K-fold cross-validation, as determined using KGE criterion. Blue values indicate good performances, while red values indicate poor performances. Grey polygons display the geographic boundaries of the major river basins.

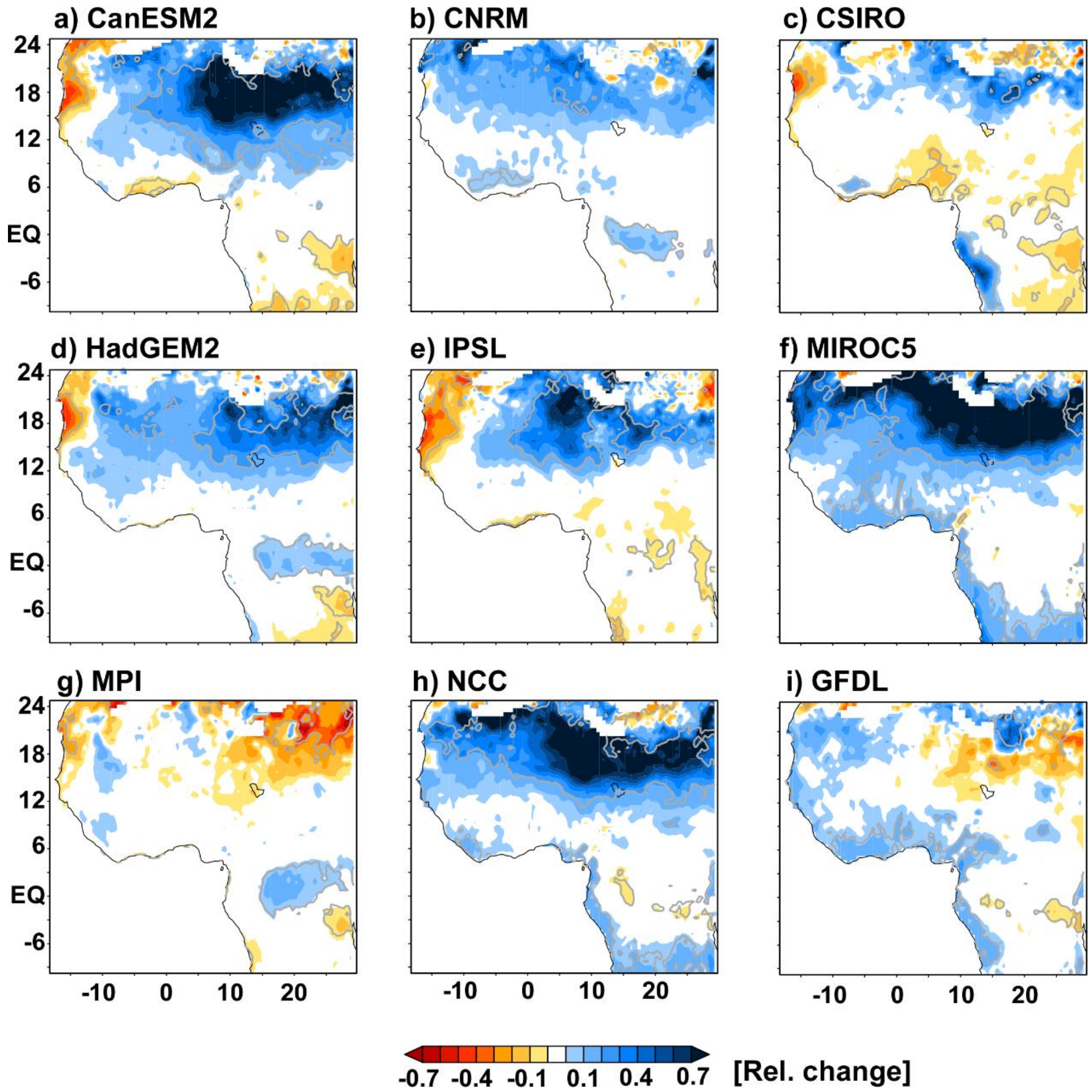

Figure 10: Near-term (2020-2050) relative change in precipitation under RCP4.5 emission scenario (a) CanESM2 (b) CNRM (c) CSIRO (d) HadGEM2 (e) IPSL (f) MIROC5 (g) MPI (h) NCC (i) GFDL. White colour corresponds to relative changes of ± 0.05. Grey contours highlight regions of significant changes (p≤0.1) based on a t test, applied for each grid-point.

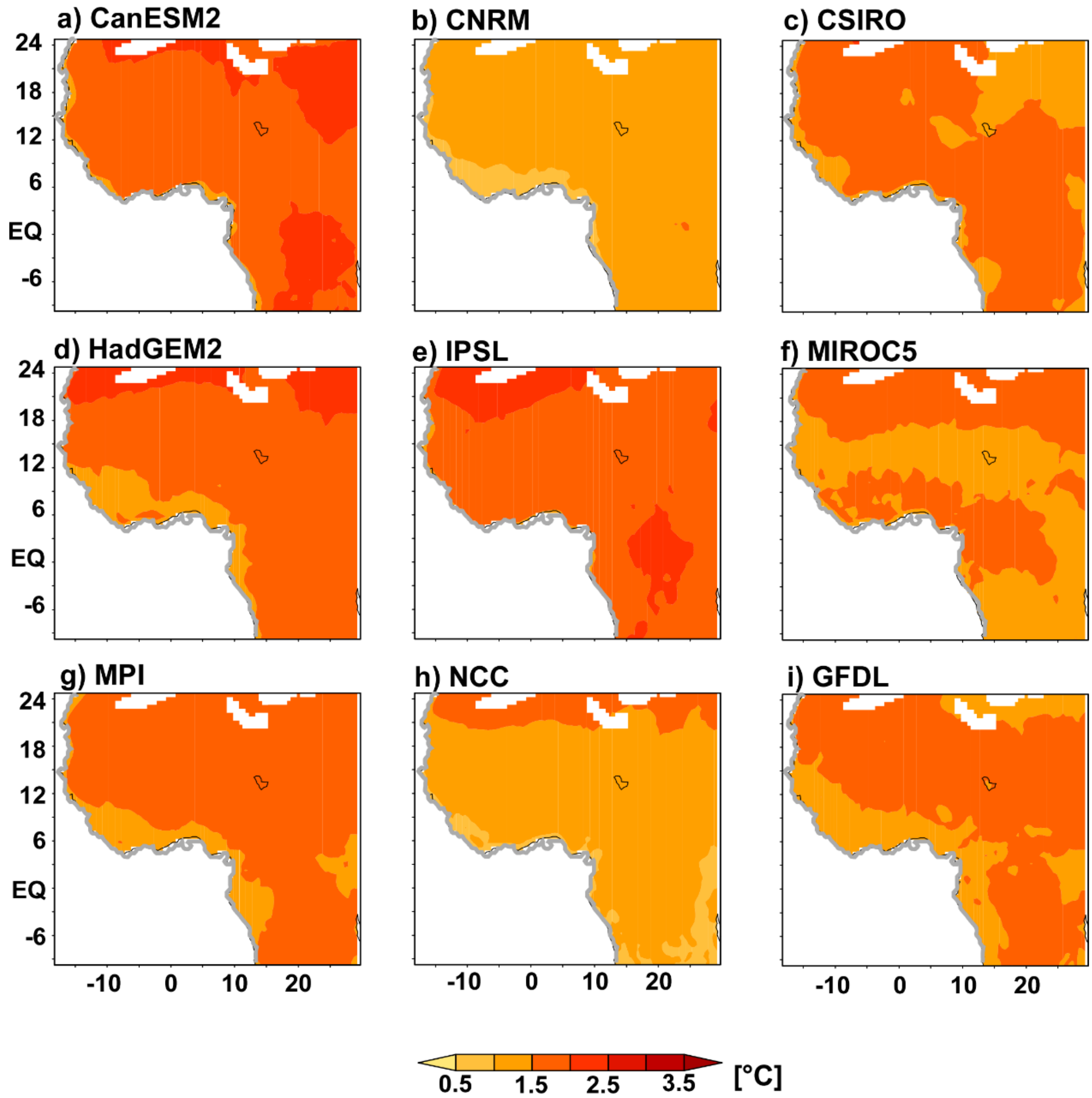

Figure 11: Near-term (2020-2050) absolute changes in maximum temperatures under RCP4.5 emission scenario (a) CanESM2 (b) CNRM (c) CSIRO (d) HadGEM2 (e) IPSL (f) MIROC5 (g) MPI (h) NCC (i) GFDL. Grey contours highlight regions of significant changes (p<0.1) based on a t test, applied for each grid-point.

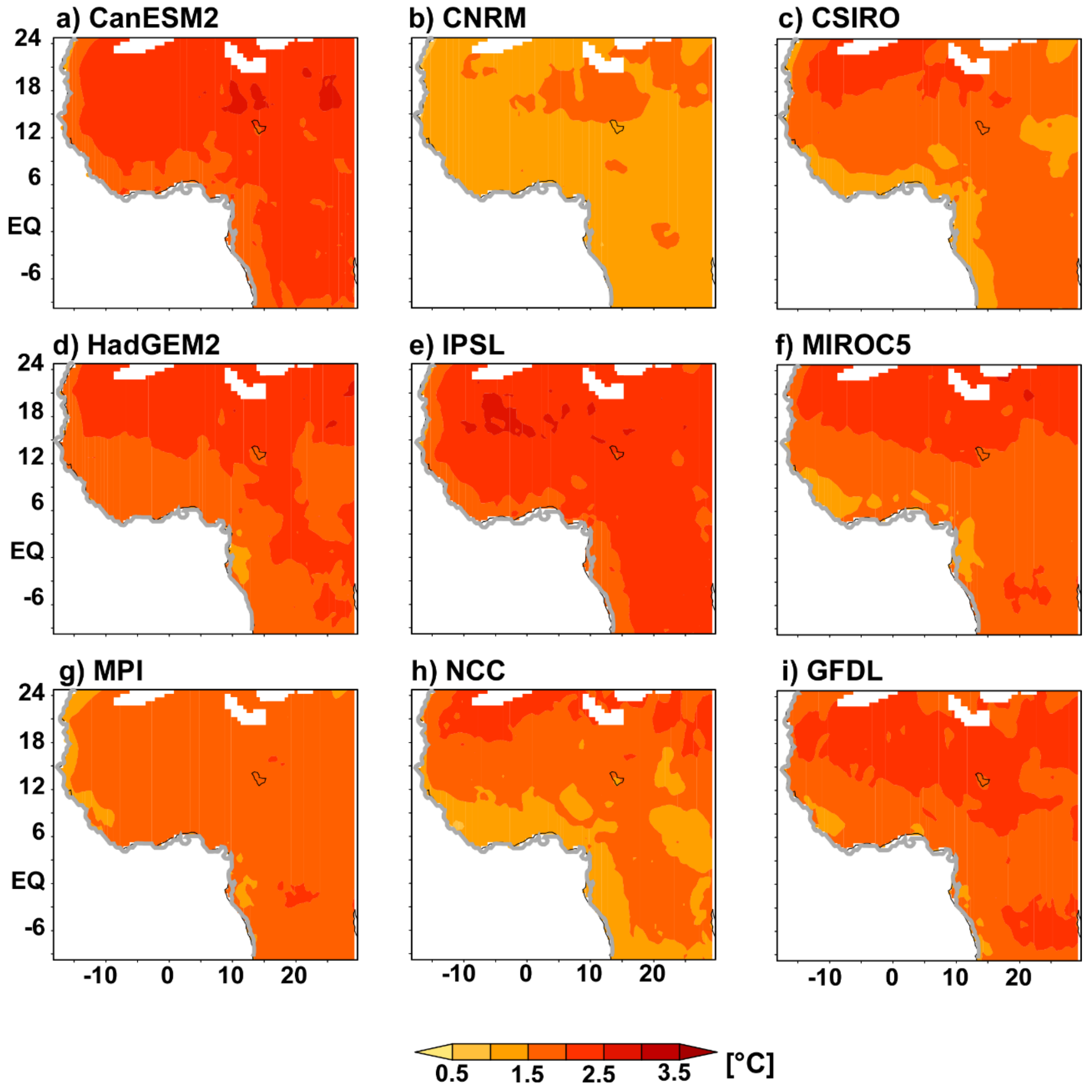

Figure 12: Near-term (2020-2050) absolute changes in minimum temperatures under RCP4.5 emission scenario (a) CanESM2 (b) CNRM (c) CSIRO (d) HadGEM2 (e) IPSL (f) MIROC5 (g) MPI (h) NCC (i) GFDL. Grey contours highlight regions of significant changes (p<0.1) based on a t test, applied for each grid-point.

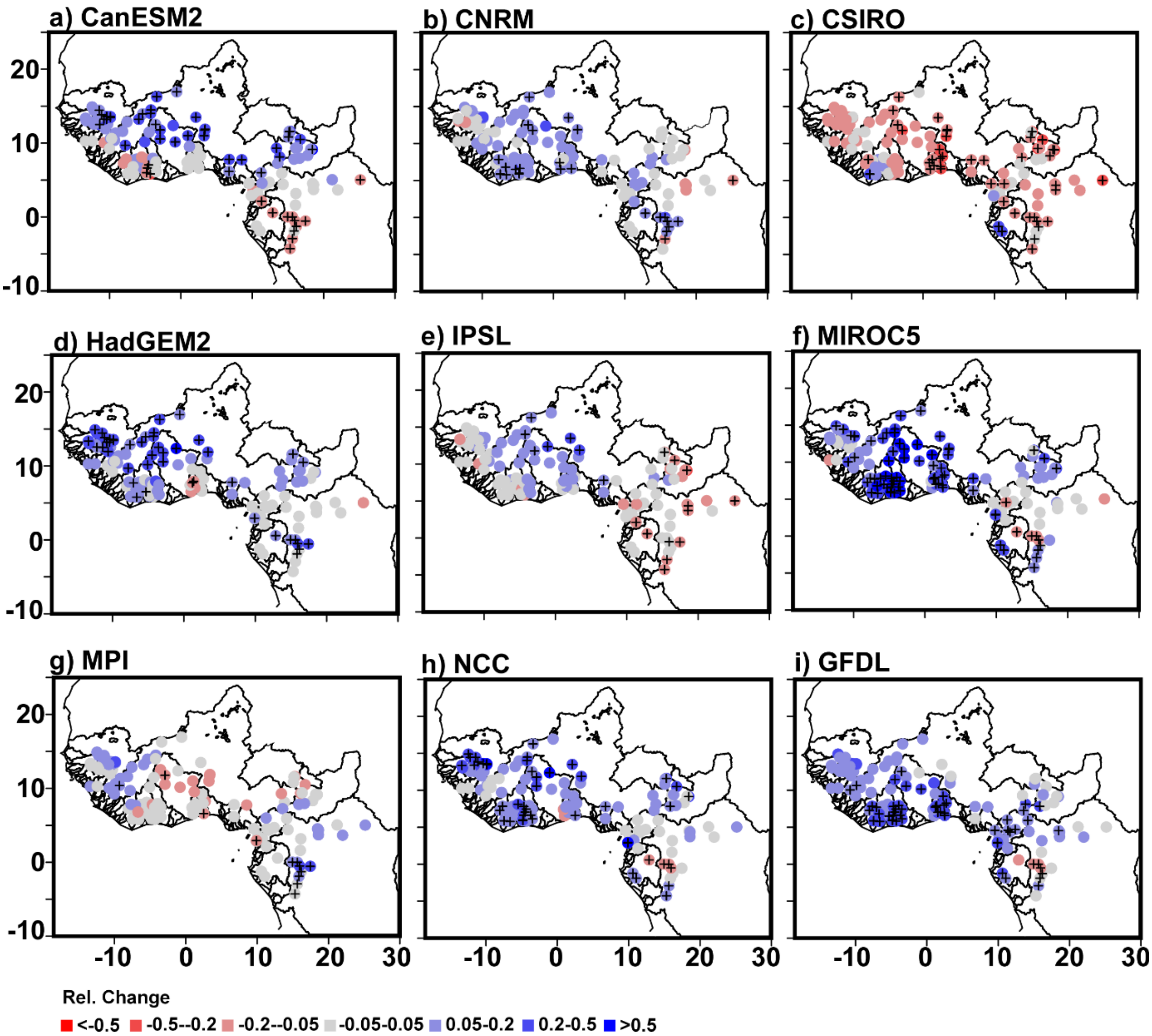

Figure 13: Near-term (2020-2050) relative change in discharge for the GR2M model under RCP4.5 emission scenario (a) CanESM2 (b) CNRM (c) CSIRO (d) HadGEM2 (e) IPSL (f) MIROC5 (g) MPI (h) NCC (i) GFDL. Black crosses highlight regions of significant changes (p≤0.1) based on a t test.

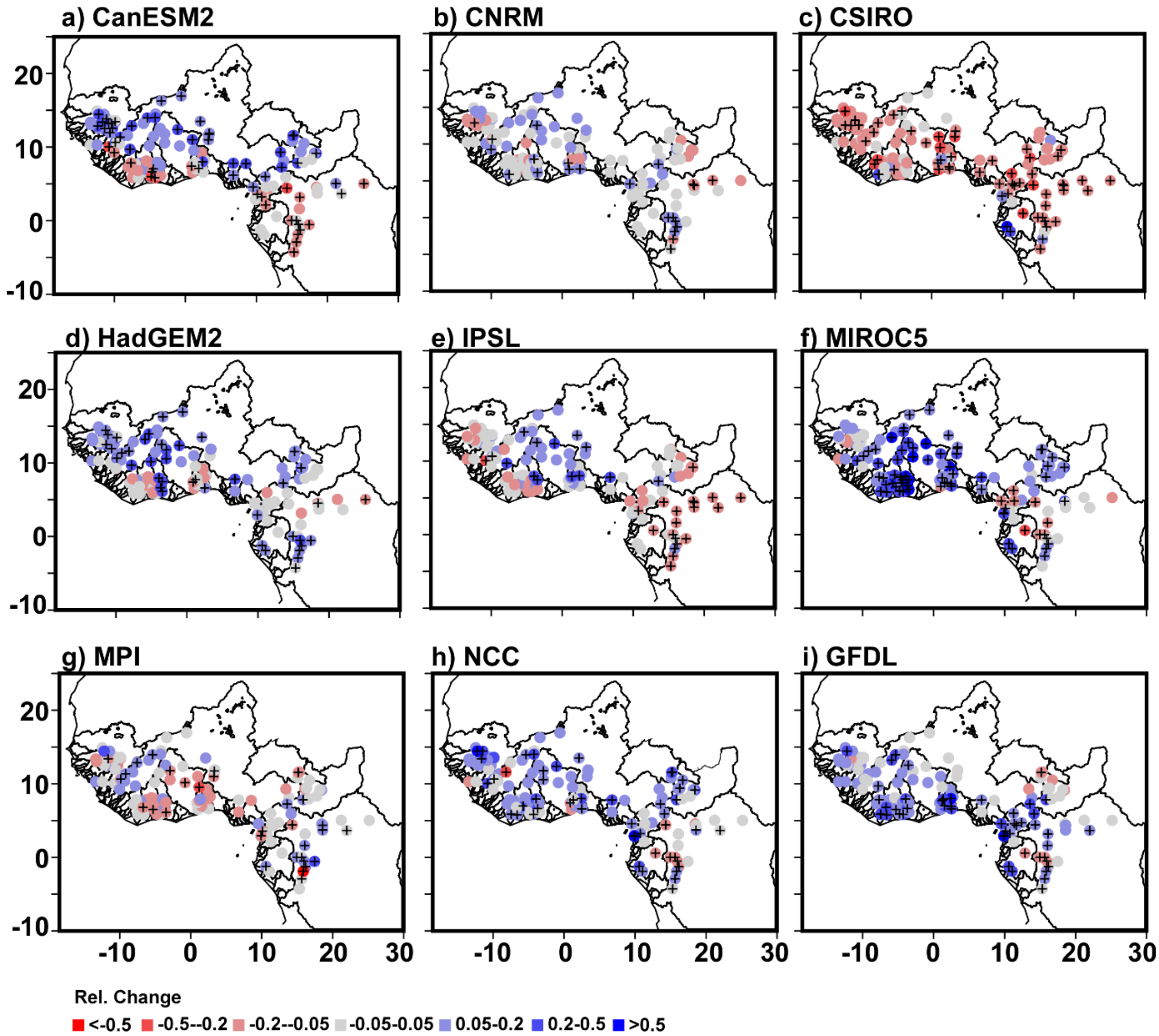

Figure 14: Near-term (2020-2050) relative change in discharge for the IHACRES model under RCP4.5 emission scenario (a) CanESM2 (b) CNRM (c) CSIRO (d) HadGEM2 (e) IPSL (f) MIROC5 (g) MPI (h) NCC (i) GFDL. Black crosses highlight regions of significant changes (p≤0.1) based on a t test.

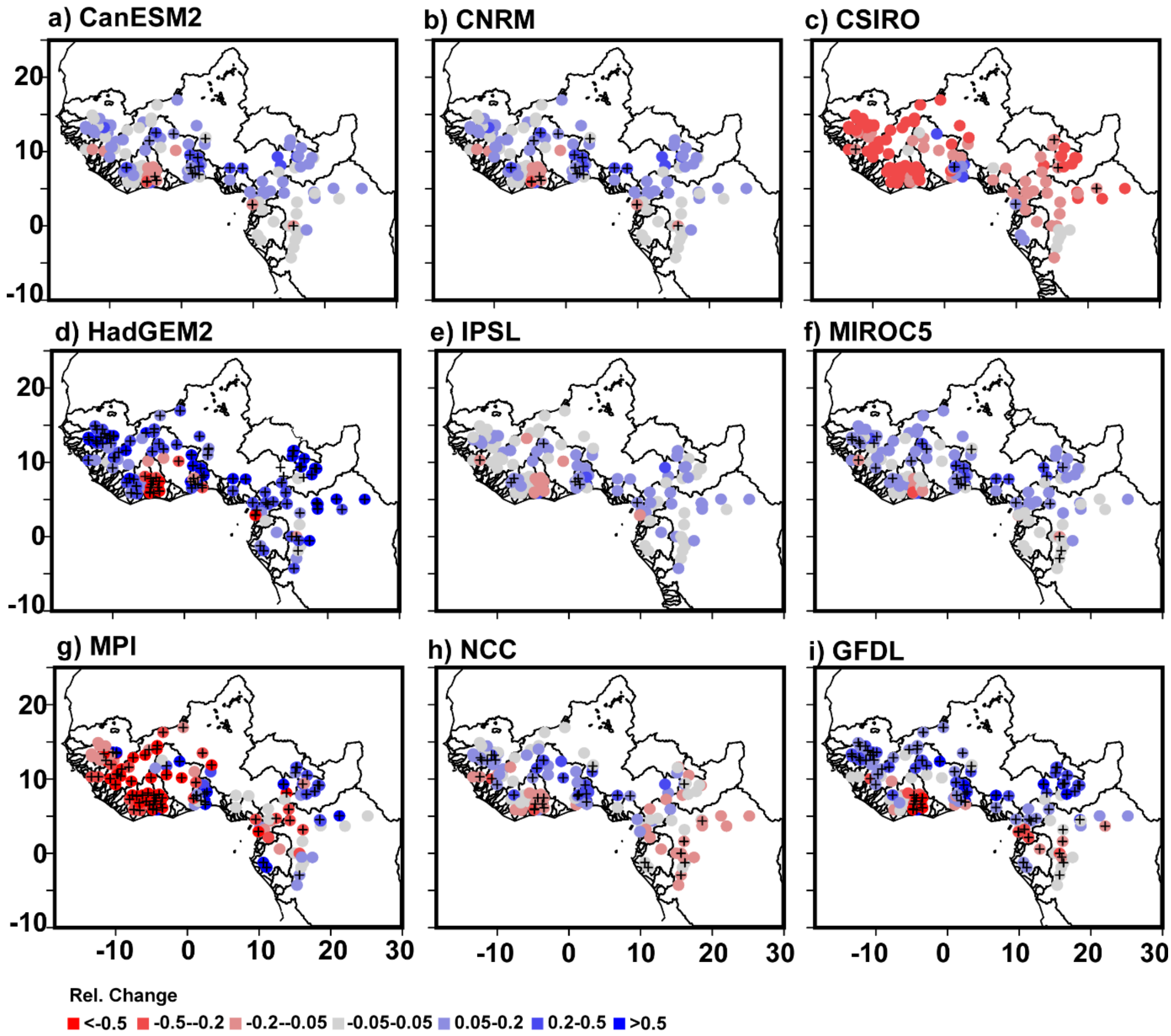

Figure 15: Near-term (2020-2050) relative changes in discharge for the teleconnections-based linear regression model under RCP4.5 emission scenario (a) CanESM2 (b) CNRM (c) CSIRO (d) HadGEM2 (e) IPSL (f) MIROC5 (g) MPI (h) NCC (i) GFDL. Black crosses highlight regions of significant changes (p≤0.1) based on a t test.

Supplementary materials

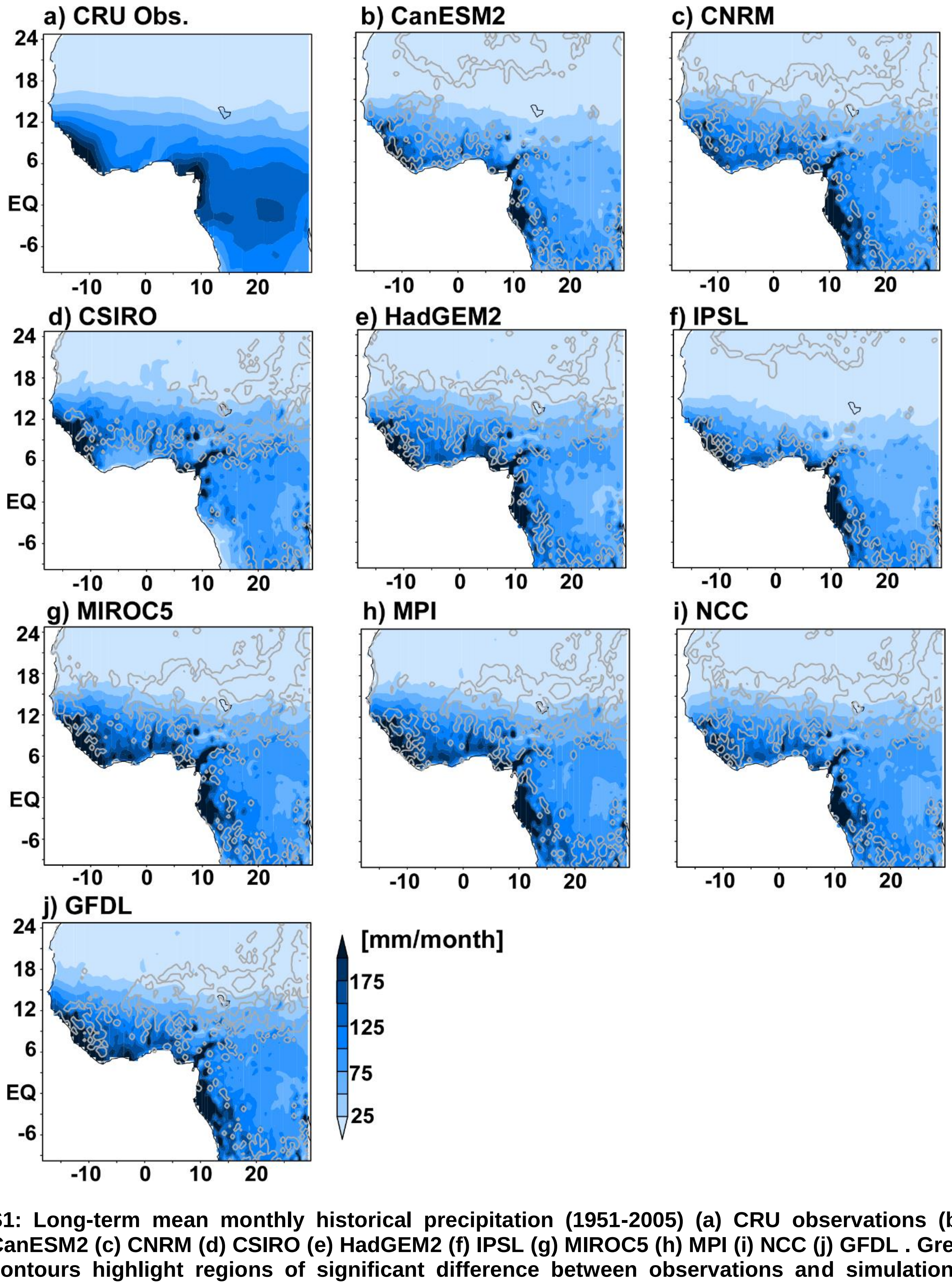

S1: Long-term mean monthly historical precipitation (1951-2005) (a) CRU observations (b) CanESM2 (c) CNRM (d) CSIRO (e) HadGEM2 (f) IPSL (g) MIROC5 (h) MPI (i) NCC (j) GFDL . Grey contours highlight regions of significant difference between observations and simulations ($p \leq 0.1$) based on a t test, applied for each grid-point.

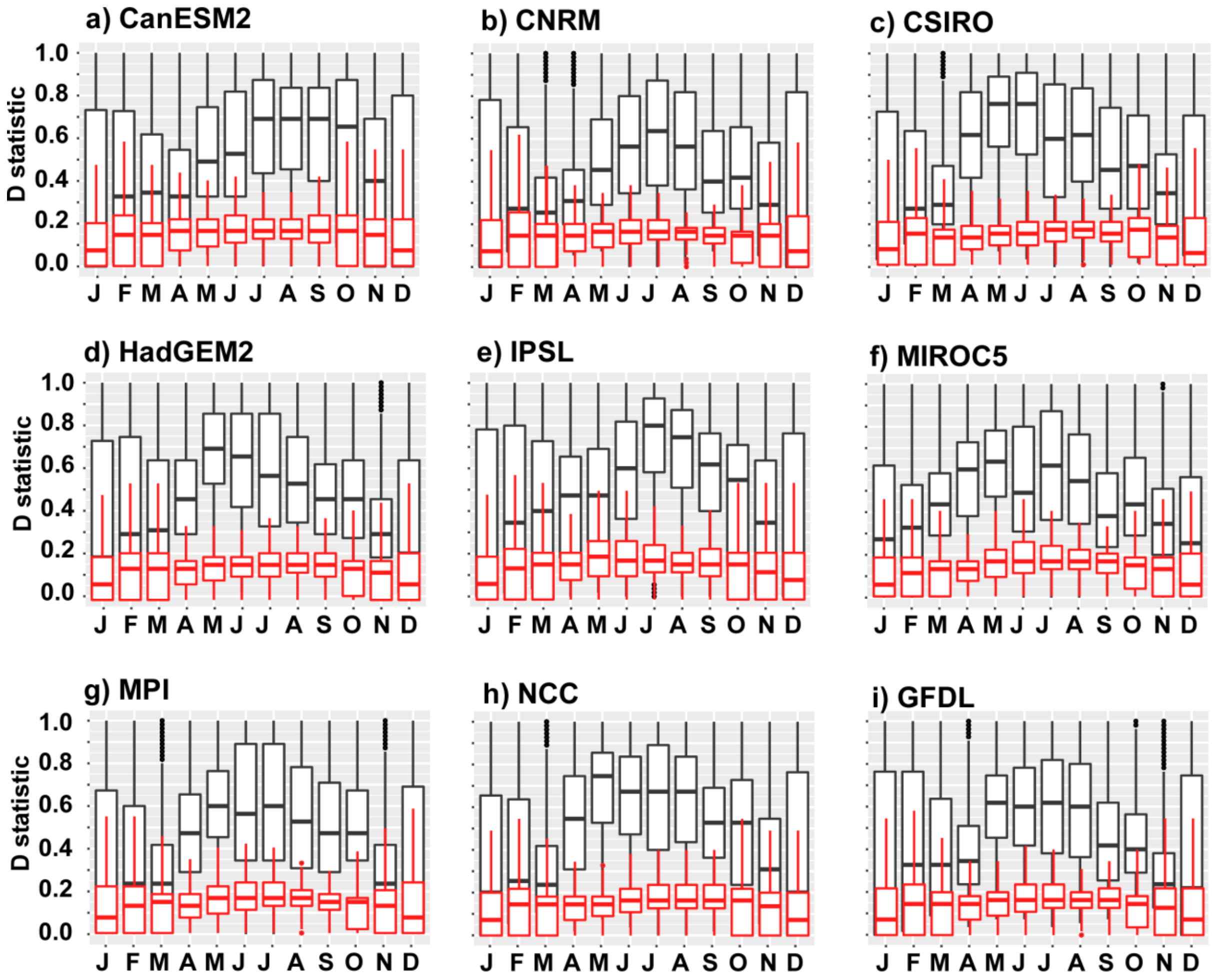

S2: Seasonal distributional biases (K-S test statistic D) in historical precipitation between observation and climate model simulations for the period 1951-2005. White boxplots correspond to historical simulations and red boxplot correspond to bias-corrected (cross-validation) simulations. (a) CanESM2 (b) CNRM (c) CSIRO (d) HadGEM2 (e) IPSL (f) MIROC5 (g) MPI (h) NCC (i) GFDL. At p≤0.1 the critical value is 0.1645.

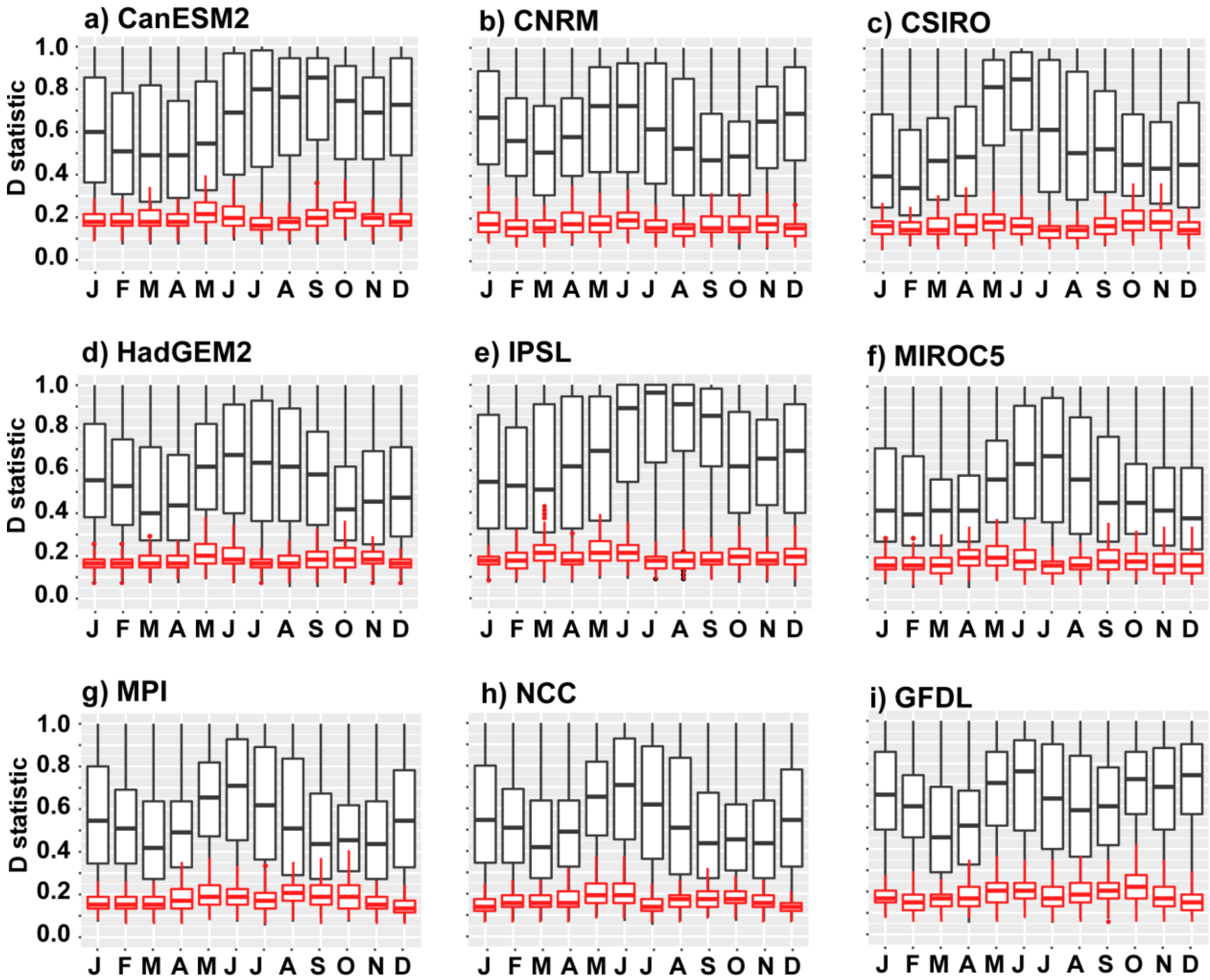

S3: Seasonal distributional biases (K-S test statistic D) in historical maximum temperatures between observation and climate model simulations for the period 1951-2005. White boxplots correspond to historical simulations and red boxplot correspond to bias-corrected (cross-validation) simulations. (a) CanESM2 (b) CNRM (c) CSIRO (d) HadGEM2 (e) IPSL (f) MIROC5 (g) MPI (h) NCC (i) GFDL. At p≤0.1 the critical value is 0.1645.

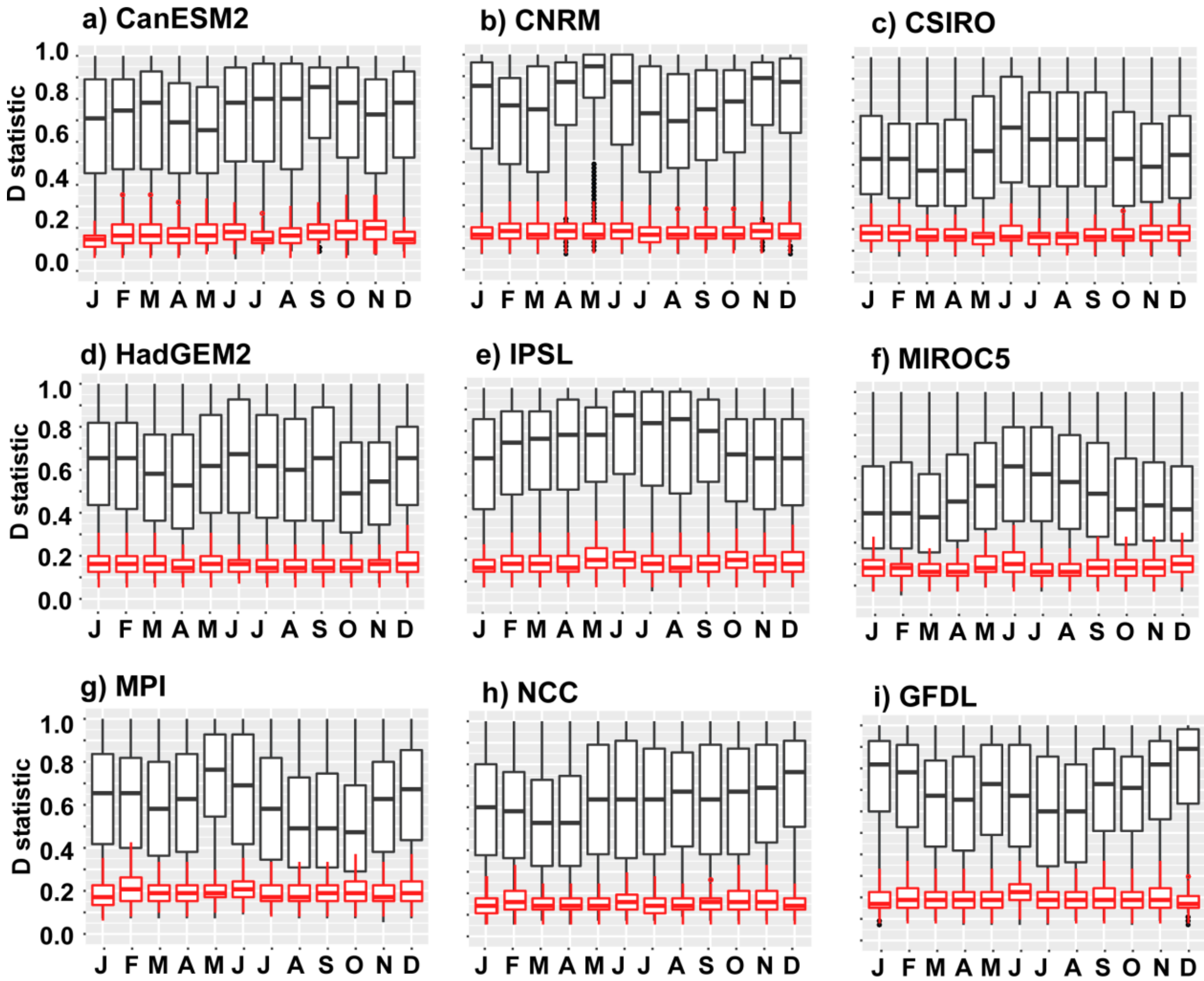

S4: Seasonal distributional biases (K-S test statistic D) in historical minimum temperatures between observation and climate model simulations for the period 1951-2005. White boxplots correspond to historical simulations and red boxplot correspond to bias-corrected (cross-validation) simulations. (a) CanESM2 (b) CNRM (c) CSIRO (d) HadGEM2 (e) IPSL (f) MIROC5 (g) MPI (h) NCC (i) GFDL. At p≤0.1 the critical value is 0.1645.

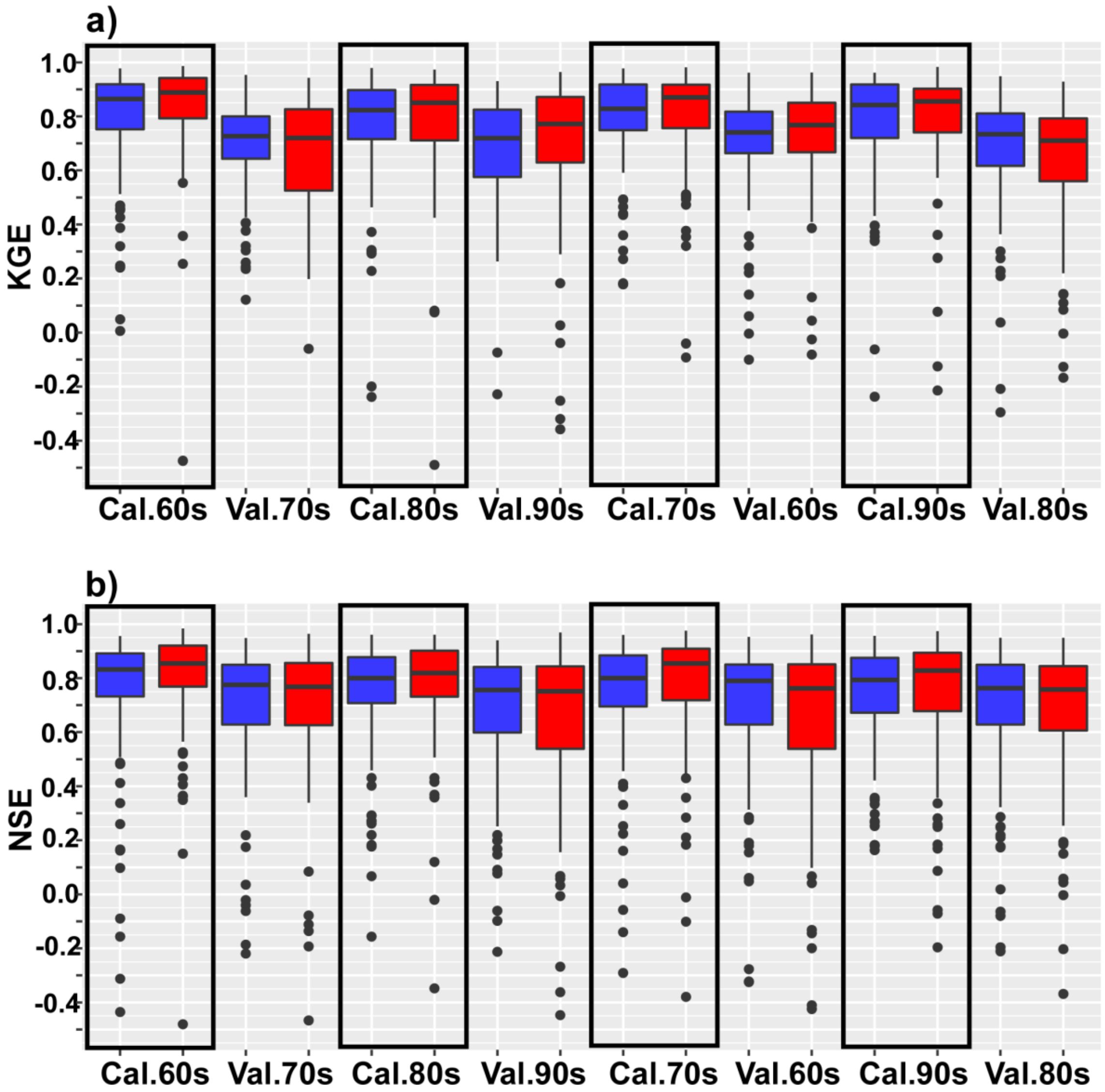

S5: Hydrological model performances for different calibration and validation periods. a) Kling-Gupta Efficiency; b) Nash-Sutcliffe Efficiency. Blue refers to GR2M and red to IHACRES-CWI.

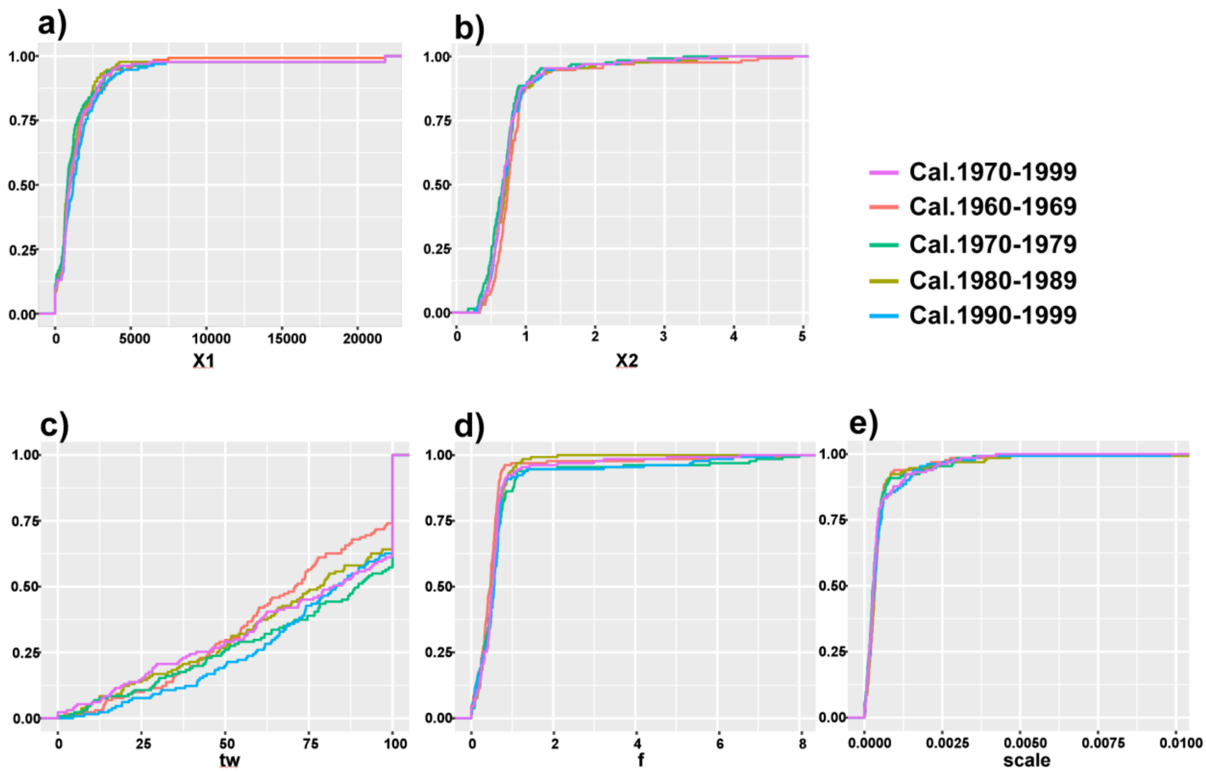

S6: Cumulated distribution functions of Hydrological model parameters for different calibration periods over the entire study area (a) GR2M X1 parameter (b) GR2M X2 parameter (c) IHACRES-CWI tw parameter (d) IHACRES-CWI f parameter (e) IHACRES-CWI scale parameter.

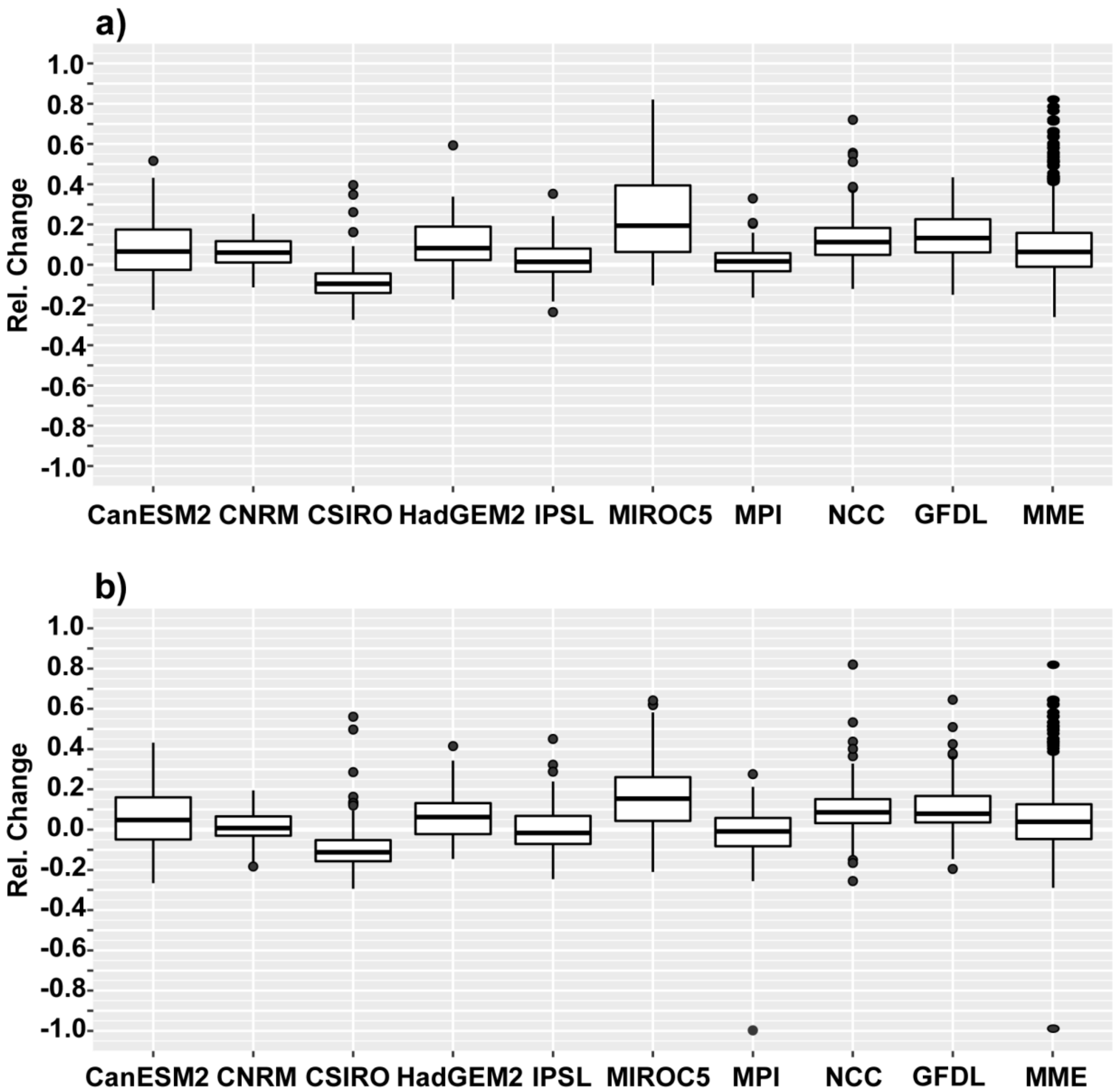

S7: Relative change in streamflow by mid-21st simulated by both hydrological models (a) GR2M (b) IHACRES-CWI.

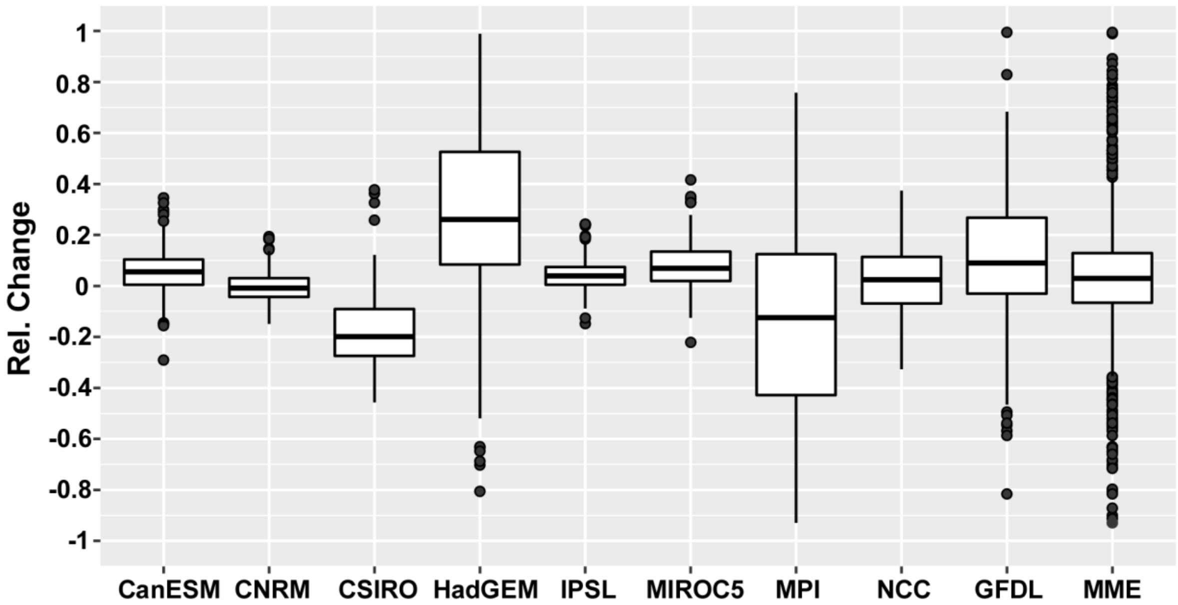

S8: Relative change in streamflow by mid-21st simulated by the multi-timescale teleconnections-based regression model.